北海道工業開発試験所報告

REPORTS OF THE GOVERNMENT INDUSTRIAL DEVELOPMENT LABORATORY, HOKKAIDO

第19号　　昭和54年3月

目　　次

— 報文 —

工業技術院

北海道工業開発試験所

横形充塡流動層分級装置の分級特性

加藤邦夫*　安達富雄**
番場克二***

横形充塡流動層を用いて 48～400 mesh のガラス粒子，28～80mesh のポリスチレン粒子，48～250 mesh のジルコンサンド粒子を分級した．その結果，本装置は粒子径が 30～400 mesh で粒子密度が 1.0～5.0 g/cc の粒子を非常に効率よく分級することがわかった．本装置での分級特性を部分分級効率で表し，部分分級効率と操作条件との間によい相関関係を見いだした．本装置を用いることによって，粒子径の差が 1.2 倍ある粒子を 80 % の効率で分級することが可能である．

1．緒　　言

粉体粒子を取り扱う操作は各種工業で広く行われている。通常粒子はその大きさおよび形状が一様でないのが普通である．そこで，粒子径分布をもった粒子群を分級して粒子径を揃えることが工業上重要な操作となる．

ところで，粒子を分級するには，ふるい，重力式分級機，遠心式分級機，慣性力式分級機など種々のタイプの分級機が用いられているが，粒径の広い範囲にわたって能率よく，かつ優れた分級特性を持った分級機はまだ考案されていないようである．

すでに著者らは充塡流動層分級装置[1]および多段スクリーン形分級装置[2]などを考案し，それらの分級特性を調べたところ，いずれもかなり優れた分級装置であることがわかった．しかし，すでに報告した充塡流動層分級装置[1]では装置内での粒子の滞留時間が比較的短いので分級と他の操作，たとえば粒子の乾燥とか，固－気反応，活生炭の再生などを併用して行うことが不可能である．また，分級における粒子の処理能力は塔断面積に比例するので，塔断面積を広くした方がより粒子を効率的に処理することが可能である．一方，多段スクリーン形分級装置[2]は非常に優れた分級特性を持っているが，装置規模を大きくした場合にその分級性能を保つためには装置各段面のスクリーン上で流体が一様に流れるよう工夫しなければならない．

以上の点を改良したのが横形充塡流動層分級装置である．この分級装置での分級特性の概略はすでに報告した[3]すなわち，本装置の分級特性を本装置上部粒子取り出し口基準の部分分級効率 βi で表し，βi に影響を及ぼすと考えられる諸因子(塔の高さ L，粒子の供給・排出の位置 L_B および L_F) と分級特性との間の関係を調べたところ，充塡物径が1.3～3.6 cm程度でフリーボードが15 cm 以上あり，かつ流動化層高が5 cm以上あり，かつ粒子の滞留時間が 5 分以上あればそれらの因子は分級特性にはほとんど影響を及ぼさないことがわかった．そこで，本研究では充塡物の形状に金網リングおよびラシヒリングを用いた場合の分級特性を調べる．次に分級する粒子をガラス粒子のほか，ポリスチレン粒子，ジルコンサンド，活性アルミナなど密度差の異なる粒子を分級し，その分級特性を調べる．また粒子の供給速度を変えて，本装置の分級処理能力についても調べてみた．以上の実験に基づいて本装置での分級特性と操作条件との間によい相関関係を得たのでここに報告する．

2．実験装置および実験方法

実験装置は **Fig. 1** に示す．装置本体は縦 8 cm 横 10 cm の矩形の断面を持つ塔および縦 8 cm 横 20 cm の矩形の断面を持つ塩化ビニール製の塔である．塔の高さはフランジ接続部を取り付けたり，取りはずしたりすることによって約 30cm，50 cm，80 cm の 3 段階に変えられる．使用した充塡物は **Table 1** に示す．すなわち，直径と高さのほぼ等しい円筒形のカナアミリングで，その大きさは球相当径 Dp=1.29～3.61 cm のものを用いた．そのほかに Dp=2.29 cm のラシヒリングも用いた．気体分散板としては開孔比，1.0%，穴径 1mm の多孔板を用いた．分級に使用した粒子群を **Table 2** に示す．すなわち，密度が 1.0 g/cc 程度のポリスチレン粒子から 4.6 g/cc のジルコンサンド粒子を用いた．

実験にあたってはあらかじめ流量を測定した空気を気体分散板を通して塔内に供給すると同時に粒子径分布の測定してある粒子をホッパーより塔内に供給する．塔内へ供給された粒子は充塡流動層内の均一で激しい流動化により分級が起こる．塔内空筒基準ガス速度に比べて比

※　郡馬大学工学部化学工学科
※※　北海道工業開発試験所第3部第3課
※※※　河西工業㈱

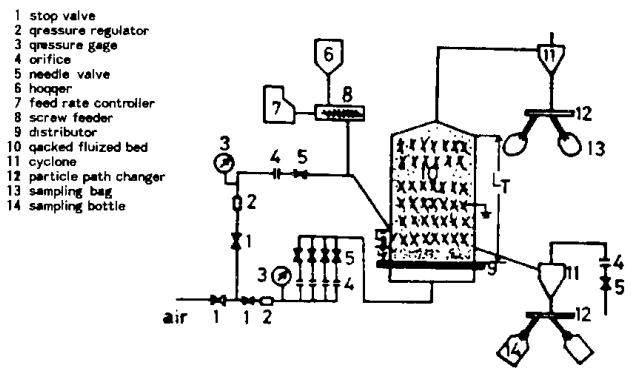

Fig. 1 Experimental apparatus

Table 1 Packing used in this experiment

Packing	Sign	Screen opening [μ]	d[cm]	h[cm]	D_p[cm]	ε[cm]
Cylindrical screen packing	PN-1	1,000	1.15	1.06	1.28	0.96
	PN-3	1,680	1.43	1.30	1.59	0.967
	PN-5	1,000	1.80	1.80	2.06	0.975
	PN-9	4,000	2.00	2.54	2.48	0.99
	PN-7	7,600	2.73	4.22	3.61	0.99
Raschigring	—	—	2.00	2.00	2.29	0.74

Table 2 Particles used in this experiment

	d_p [mesh]	d_p av [μ]	X_i [—]	U_{Tio} [cm/sec]
Glass particle	− 48+ 60	274	0.036	226.5
	− 60+ 80	184	0.262	152.6
	− 80+100	163	0.126	136.0
A	−100+115	137	0.200	118.7
	−115+150	115	0.108	69.4
	−150+170	97	0.126	59.4
	−170+200	81	0.086	45.5
	−200+250	67	0.056	37.5
Glass particle	−115+150	115	0.08	69.4
	−150+170	97	0.163	59.4
	−170+200	81	0.245	45.5
B	−200+250	67	0.292	37.5
	−250+270	58	0.118	31.0
	−270+325	48	0.071	23.0
	−325+400	40	0.031	15.0
Polystyrene particle	− 28+ 32	545	0.103	
	− 32+ 36	460	0.284	
	− 36+ 42	385	0.111	
	− 42+ 48	316	0.233	
	− 48+ 60	274	0.046	
	− 60+ 70	230	0.127	
	− 70+ 80	210	0.096	
Zircon sand	− 48+ 60	274	0.027	
	− 60+ 80	184	0.102	
	− 80+100	163	0.095	
	−100+115	137	0.226	
	−115+150	115	0.277	
	−150+270	97	0.166	
	−170+200	81	0.097	
	−200+250	67	0.010	
Activated alumina	− 48+180	237	0.546	
	− 80+100	163	0.119	
	−100+115	137	0.132	
	−115+250	115	0.102	
	−150+200	90	0.084	
	−200+250	67	0.017	

較的小さい終末速度をもつ粒子は塔内を上昇し，粒子上部取り出し口に捕集される．一方，塔内ガス流速に比べて比較的大きな終末速度をもつ粒子は，粒子供給口から最も離れた位置に取り付けた粒子取り出し口より捕集される．実験開始後上記の二つの粒子取り出し口より一定時間間隔で粒子を捕集し，各取り出し口でのその重量が一定になることにより分級が定常状態になったことを確認した．各粒子取り出し口より流出する粒子質量速度を測定することにより本装置への粒子供給速度を求めた．また捕集粒子の一部を **JIS** 標準フルイでふるいわけして各粒子組成を分析した．

本装置内での静電気の発生をできるだけ防ぐために充填物からはアースをとった．

3．実 験 結 果

本装置の分級特性を装置上部粒子取り出し口基準の部分分級効率 β_i で表す．すなわち

$$\beta_i = \frac{A Y_i}{F_0 X_i} \qquad (1)$$

本実験においては前報[3]においてすでに報告した装置的条件が分級特性に影響を及ぼさない領域で分級特性を調べてみた．

まず，充填物の形状が分級特性にどのような影響を与えるかを調べるため，充填物として直径 2 cm，長さ 2 cm のラシヒリング充填物を用いてガラス粒子を分級し，部分分級効率 β_i と操作ガス流速 U とをプロットしたのが **Fig. 2** である．同じ程度の大きさの金網リング充填物を用いてガラス粒子を分級した結果を **Fig.3**に示す．**Fig.2, Fig.3** において部分分級効率が 0.5 となる操作ガス流速を本装置における粒子径 d_p なる粒子のみかけの終末速度 U_{T_i} と定義する．**Fig.4**は 60mesh から 115 mesh までの粒子に対して充填物がラシヒリングの場合と同一の大きさの金網リングを用いた場合での β_i と U/U_{T_i} とをプロットしたものである．**Fig.4** よりラシヒリングのような中空の充填物を用いるより，金網リングを用いたほうがよい分級特性を示すことがわかる．ラシヒリングのようなタイプの充填物を用いると充填物の内側の空間にガス流速の遅い部分を生じ，分級性能を悪くするものと思われる．また，ラシヒリング，球などは金網リングに比べて装置単位断面積あたりの粒子の流動化面積が小さいので装置単位断面あたりの粒子の処理量が小さくなる．以上の点から充填物としては金網リングなどのような充填物間の空間率の大きなものが望ましいと思われる．そこで以下の実験では充填物として金網リングを用いた．

本装置での単位時間あたりの粒子の処理量と分級特性との間の関係を調べるために 48～250mesh の粒径分布

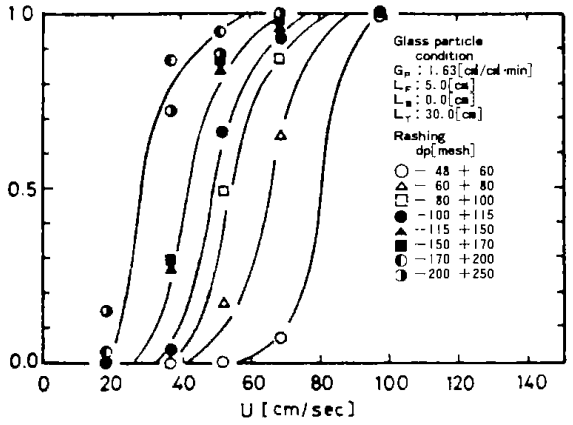

Fig. 2 Relation between U and β_i in the case of Raschig-ring packing

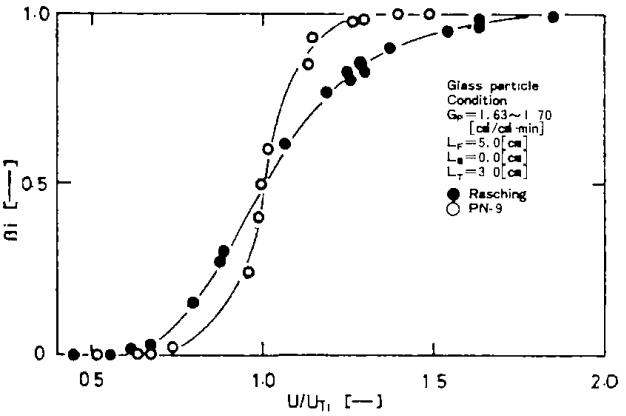

Fig. 4 Relation between U/U_{T_i} and β_i

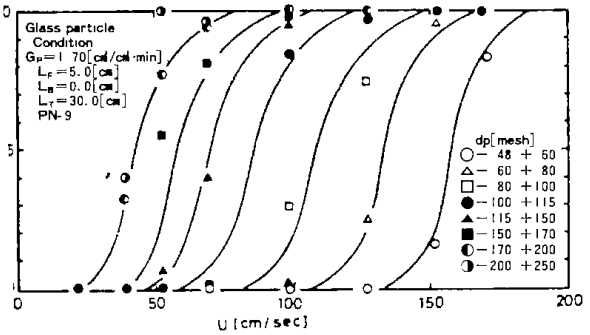

Fig. 3 Relation between U and β_i in the case of cylindrical screen packing

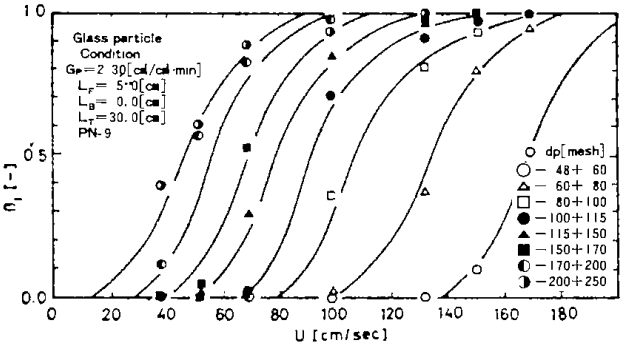

Fig. 5 Relation batween U and β_i at G_p 2.3cc/cm². min

を持ったガラス粒子を種々の供給速度で本装置に供給し，供給速度の分級効率に及ぼす影響を調べてみた．さきの **Fig. 3** は装置単位断面あたりの粒子供給速度 G_p が 1.7 cm³/cm²·min の時の β_i と U との関係を粒子径 d_p をパラメータとして示したものである．一方 **Fig. 5** は G_p が 2.3 cm³/cm²·min の場合での β_i と U との関係を示したものである．**Fig. 3** および **Fig. 5** において粒子径が 60～100 mesh の粒子に対して β_i と U/U_{T_i} とをプロットしたのが **Fig. 6** である．**Fig. 6** より粒子供給速度が 1.7 cm³/cm²·min より大きくなると分級特性が多少悪くなっていることがわかる．なお，1.7 cm³/cm²·min 以下の供給速度では分級特性は粒子の供給速度によってほとんど影響を受けなかった．さらに粒子密度の異なる粒子を用いて粒子の供給速度による分級特性への影響を調べたところほぼ同じ結果が得られた．本装置での粒子の分級速度は流動化粒子層表面からの粒子の飛び出し速度に比例すると考えられるので装置断面積が分級粒子の処理量に最も影響を及ぼす因子ではあるが，その他に粒子の流動化層高とか，装置の縦，横比などによっても粒子の処理量は影響されるものと思われるので，本実験で得られた粒子処理量に対する知見は，本装置で分級を行う場合の一応のめやすと考えるべきである．このように分級特性に影響を与えない最大の粒子供給速度をこの装

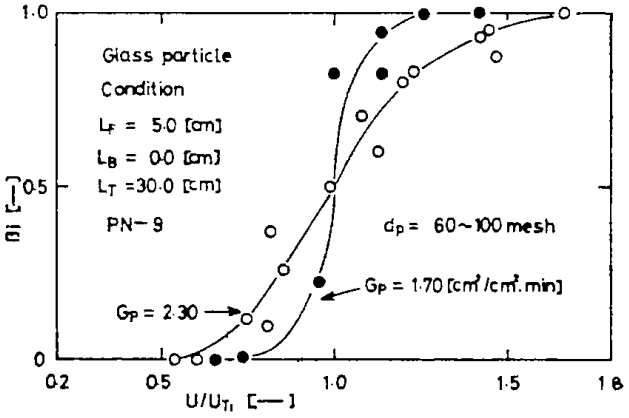

Fig. 6 The effect of feed rate upon β_i

置における限界粒子供給速度と定義する．この限界粒子供給速度以内で粒子を処理した場合，一定操作ガス流速のもとで，装置下部粒子取り出し口より取り出される各粒子組成と流動化粒子層でのそれとほぼ一致した．

次に分級粒子の密度の分級特性に及ぼす影響を調べるため密度の大きいジルコンサンド粒子(ρ_p =4.6 g/cc)と密度の小さいポリチスレン粒子 (ρ_p=1.03 g/cc)を本装置で分級し，分級特性を調べてみた．**Fig. 7** はジルコンサンド粒子を分級した場合の部分分級効率 β_i と粒子径 d_p との関係を操作ガス流速をパラメータとして示したもの

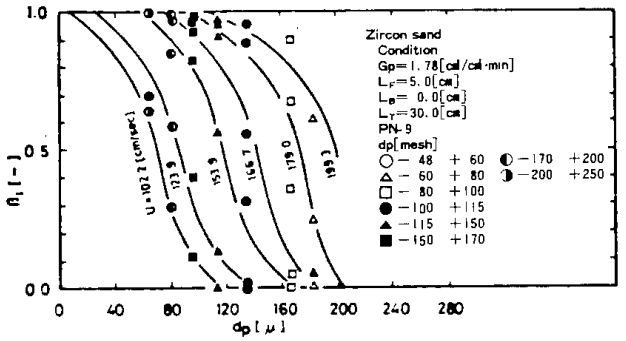

Fig. 7 Relation between d_p and β_i in the case of zircon sand

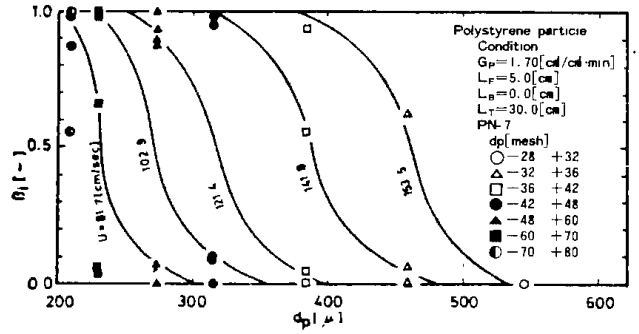

Fig. 8 Relation detween d_p and β_i in the case of polystyrene particles

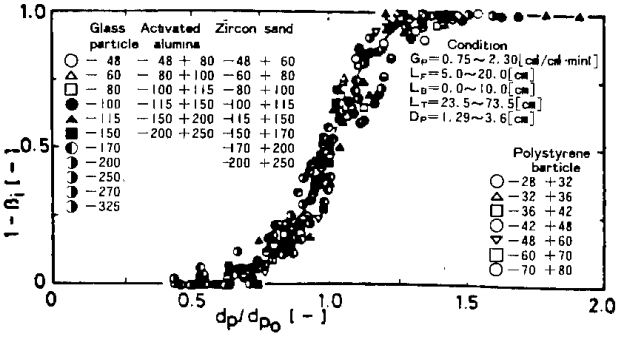

Fig. 9 Relation between d_p/d_o and $1-\beta$

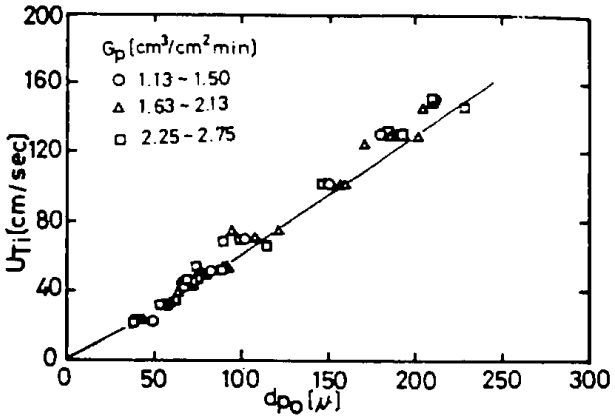

Fig. 10 Relation batween d_{po} and U_{T_i}

である．**Fig.8** はポリスチレン粒子を分級した場合のβ_iと d_p とを操作ガス流速をパラメータとして示したものである．**Fig. 7** および **Fig.8** において，各操作ガス流速における部分分級効率が 0.5 となる粒子径をその操作ガス流速における標準分級粒子径 d_{p0} と定義する．

ところで本装置での分級特性に関する一般的相関を得るため，一定操作ガス流速のもとでの標準分級粒子径 d_{p0} と各粒子径の比 d_p/d_{p0} と下部粒子取り出し口基準の部分分級効率 $(1-\beta_i)$ とをプロットしたのが**Fig.9**である．**Fig.9** より本装置では粒子供給速度が 1.7cm³/cm²·min 以下であれば粒子径，粒子密度などに関係なくよい相関が得られることがわかる．**Fig. 9** より $d_p=0.9d_{p0}$ の粒子および $d_p=1.1d_{p0}$ の粒子の β_i は 0.8 および 0.2である．すなわち，横形充填流動層分級装置では粒子径が30～400mesh で粒子密度が1.0～5.0g/ccの粒子に対しては粒子径の比が約1.2倍あれば 80% の効率で粒子を分級することが可能である．

Fig. 10 はほぼ完全な球形粒子であるガラス粒子に対する本装置のみかけの終末速度 U_{Ti} と標準分級粒子径 d_{p0} とをプロットしたものである．実線はこの粒子の真の終末速度である．**Fig. 10** より本装置における各粒子のみかけの終末速度 U_{T_i} はその粒子の真の終末速度で近似することができると思われる．

Fig.9 および **Fig. 10** を用いて操作条件より本装置の分級特性を推定することができる．

4．考　　察

本分級装置において粒子供給口より投入された粒子は流動化粒子層の中へ速やかに分散する．充填流動層内での一様な激しい気泡の運動により細かい粒子は流動化層表面よりフリーボード内に投入され，上部粒子取り出し口に捕集されるのがよく観察される．充填流動層内での気泡の頻度は多くても気泡径が小さいので流動化層表面での気泡の爆発によって粒子を層表面より遠くまで飛び出すことはないので分級装置でのフリーボードを大きくとる必要はない．層内での気泡の挙動に立脚した多成分粒子の層からの飛び出し速度より分級特性を解析するのは今後の問題となる．

さて，本分級装置で粒子を分級するにあたっては，層内で粒子がよく流動化することが前提となるので粒子の形状は球形に近いほどよく，かつ粒子自体に付着性の強い粒子はこの方法での分級に適していない．本装置を用いて粒子を分級する場合，粒子径があまり大きくなると（たとえば 20 mesh 以上）それらの粒子の終末速度程度のガスを装置内に流入しなければならなくなるので送風機のコストを高めることになる．したがって，粒子径のあまり大きな粒子の分級にも本装置は適当でない．一方，粒子径を小さくすると粒子が付着しやすくなり，かつ静電気が起こりやすくなる．そこでこれらを防止して，

Table 3 Some exsamples of horizontal packed fluidized particle classifier

d_p [mesh]	Feed rate [kg/min]	First tower operating condition U =48cm/sec β_i [−]	Ayi [kg/min]	$F_0x_i - Ay_i$ [kg/min]	Second tower operating condition U =125 cm/sec β_i [−]	Ay_i [kg/min]	$F_0x_i - Ayi$ [kg/min]
− 48+ 60	10.0	0	0	10.0	0	0	10.0
− 60+ 80	10.0	0	0	10.0	0.17	1.7	8.3
− 80+100	10.0	0	0	10.0	0.5	5.0	5.0
−100+115	10.0	0	0	10.0	0.84	8.4	1.6
−115+150	10.0	0	0	10.0	1.0	10.0	0
−150+170	10.0	0.1	1.0	9.0	1.0	9.0	0
−170+200	10.0	0.5	5.0	5.0	1.0	5.0	0
−200+250	10.0	0.88	8.8	1.2	1.0	1.2	0
−250+270	10.0	1	10	0	1.0	0	0
−270+325	10.0	1	10	0	1.0	0	0
	100.0		34.8	65.2		40.3	24.9

できるだけ鋭い分級を行うには挿入空気の温度および湿度調整が必要である．以上のことより，本装置での分級に適当な粒子径は大略 20～400 mesh 程度と思われる．本装置での単位時間あたりの粒子の処理量については必ずしも解明されたわけでなはいが，この程度の粒子供給負荷（1.7 cm³/cm²·min以下)ならば，**Fig. 9** に示す程度の分級ができることを意味するものである．したがって，分級の精度を落とせば粒子供給負荷をかなりあげることが可能であるので各種工業においてはその点を考慮して本装置の設計を行うことが望ましい．

本装置はさきの充填流動層分級装置[1] に比べて細かい粒子での分級に優れているのみならず，他の操作と併用することができる利点をもつ．たとえば，分級と乾燥とを同時に行う場合，流動化層高，フリーボードの高さおよび粒子供給口と粒子取り出し口との距離を変えることによって種々の設定条件のもとで分級と乾燥とを同時に行うことが可能である．

本分級装置を2基および3基用いることによって，粒子を3群および4群に分級することが可能である．たとえば，**Table 3** に示すように各組成に対しておのおの 10wt% からなる 48～325 mesh のガラス粒子を，毎分 100 kg/min 供給する場合，2基の本分級装置を直列に用い，第1塔下部粒子取り出し口より取り出された粒子を第2塔に供給することによって粒子を3群に分級してみる．今，第1塔および第2塔での標準分級粒子径をそれぞれ 81μ および 163μ とすると**Fig.10**より第1塔および第2塔での操作ガス流速はそれぞれ 48cm/sec, 125 cm/sec である．したがって，第1塔および第2塔での各粒子の上部粒子取り出し口基準の部分分級効率および第1塔および第2塔での上部および下部粒子取り出し口より流出する粒子の組成は **Table 3** に示すようになる．すなわち，第1塔上部粒子取り出し口より 34.8kg/min，第2塔上部および下部粒子取り出し口よりそれぞれ40.3 kg/min, 24.9kg/min の粒子が取り出される．また，第1塔および第2塔での粒子負荷がそれぞれ 100 kg/min，65.2 kg/min の粒子を分級するに必要な断面の塔をそれぞれ用いればよい．以上のようにして充填流動層分級装置を設計することができる．

5．結　　言

1)　横形充填流動分級装置は簡単な操作で粒子を効率よく分級することが可能である．

1)　本装置での部分分級効率は一定流速のもとでの各粒子と標準分級粒子径との比 d_p/d_{p0} とで良好に相関できる．

3)　本装置を用いることによって粒子径の差が1.2倍あれば約 80% の効率で 30 mesh から 400 mesh の粒子を分級することが可能である．

Nomenclature

A = flow rate of particles at the upper [g/min]
D_p = particle withdrawal point average diameter of cylindrical screen packing [cm]
d = cross sectional diameter of cylindrical screen packing [cm]
d_p = particle diameter [cm]
F_o = feed rate of particles [g/min]
G_p = volume feed rate of particles per unit cross sectional area of the tower [cm³/cm²·min]
h = length of cylindrical screen packing [cm]
L_B = vertical distance between the lower particle withdrawal point and particle feed paint [cm]
L_F = distance between gas distributor and lower particle withdrawal point [cm]
L_T = tower height [cm]
U = superfical gas velocity [cm/sec]
U_{T_i} = apparent terminal velocity of i component particles [cm/sec]
X_i = weight fraction of i component

Particles in feed [—]

Y_i = weight fraction of i component particles at upper particle withdrawal point [—]

β_i = partial separation efficiency of i component particles [—]

ρ_p = density of particles [—]

ε = packing voidage [—]

Literature cited

1) *Kato, K., Y.* Shirota and U. Ito: *Kagaku kogaku Ronbunshu,* 1, 357 (1975)
2) Kato, K., H. Kato, Y. Ebinuma and U. Ito: *J. Chem. Eng. Japan,* 9, 226 (1975)
3) Kato, K., W. Sekiguchi and M. Uemoto: *Kagaku Kogaku Ronbunshu,* 2, 621 (1976)

(1976 年11月8日受理; 化学工学協会第10回秋季大会（名古屋, 1976年10月）にて発表)

The Characteristics of Particle Classification by a Horizontal Packed Fluidized Particle Classifier

Kunio Kato, Tomio Adachi* and Katsuji Banba**

Dept. of Chem. Eng., Gunma Univ., Kiryu 376

Glass beads from 48 mesh to 400 mesh, polystyrene particles from 28 mesh to 80 mesh and zircon sand particles from 48 mesh to 250 mesh were classified by a horizontal packed fluidized particle classifier.

From this investigation, if particle size was in the range of 30 mesh to 400 mesh and particle density was in the range of 1.0 g/cc to 5.0g/cc, these particles are well classified by this classifier. The characteristics of particle classification of this classifier are expressed by a partial sepration efficiency, and good correlation between particle separation efficiency and operating condition is obtained. If particles of one size are 1.2 times larger than the others, these two sizes are classified with 80% efficiency by this classifier.

* Gunma Univ.
** Government Ind. Develop. Laborotory, Hokkaido
*** Kasai-Kogyo Co., Ltd.

(化学工学論文集、第3巻第5号 (1977), P.473～476)

THE EFFECT OF BED DIAMETER ON THE BEHAVIOR OF BUBBLES IN GAS-SOLID FLUIDIZED BEDS*

MINORU TOMITA AND TOMIO ADACHI
The Government Industrial Development Laboratory, Hokkaido; Sapporo, Japan

Behavior of rising bubbles has been studied in fluidized beds of 21.4, 37.8 and 59.9 cm I.D. Sands of mean size 0.202 mm were fluidized by air at velocities ranging up to 25 cm/sec. Bubble frequency and volume fraction of bubbles in the beds were measured with a capacitance probe. Upward and downward forces produced by fluidization were measured with a strain gage probe. Bubble diameter and rising velocity were evaluated by analyzing the experimental results.

In the level region up to about 20 cm from the distributor, bubbles coalesced rapidly, rising along the wall of the bed. Particles flowed up along the wall and flowed down through the central portion of the bed. In the region of levels higher than about 20 cm from the distributor, the behavior of bubbles was strongly affected by the wall of the bed as the bubbles grew larger. Particles flowed down along the wall and flowed up through the central portion of the bed.

1. Introduction

Many investigations have been made, mainly on a small scale, in an attempt to understand the behavior of gas-solid fluidized beds. However, little works has been reported on large-scale fluidized beds. May[7] measured the axial diffusion coefficient of solid particles in fluidized beds of 0.6–1.5 m diameter. de Groot[1] studied the effects of fluidizing air velocity, bed diameter (0.1–1.5 m), bed height (1.0–1.5 m) and size distribution of crushed silica particles on the behavior of bubbles. Whitehead *et al.*[11] investigated the behavior of bubbles in square cross section fluidized beds 1.5 m^2 in area and up to 2.4 m in depth. Kunii *et al.*[5] studied the behavior of bubbles in beds of 40 cm I.D. with micro-spherical and FCC catalysts fluidized by air. Ikeda[3] studied the synthesis of acrylonitrile by the catalytic oxidation of propylene and ammonia in fluid beds of 8–360 cm I.D. He discussed the relation between the reaction conversion and the dip-length equivalent diameter of the beds. Hovmand *et al.*[2] measured ozone conversion in a fluidized-bed reactor of 46 cm I.D. and up to 2.5 m bed height at fluidizing gas velocities up to about 30 cm/sec, using sands of 75 and 125 μ in mean diameter as fluidizing particles. They analyzed the ozone conversion data on the basis of both the slug flow model and the bubble model, and discussed the effects of bed diameter and distributor upon the ozone conversion and behavior of bubbles.

In spite of these investigations, our knowledge is still insufficient for the design or scale-up of fluidized bed reactors. Present paper is concerned with the experimental study of the scale effect on the behavior of bubbles in fluidized beds, especially in the intermediate-scale region.

2. Apparatus and Procedures

Fluidized beds of 1.0 m height and 21.4, 37.8 and 59.9 cm I.D. were used. The columns were made of polymethylmethacrylate. The distributor used in each column was made by fitting a 200-mesh screen between two plates perforated with orifices of 0.1 cm diameter in equilateral triangular arrangement with 1.5 cm pitch. Calming section was made by packing glass beads of 1.2 cm diameter just under the distributor. The air was sent to the bed through a buffer tank, an orifice flow meter, the calming section and the distributor by a roots blower. The fluidizing gas velocity was controlled by two regulation valves.

Sands of 0.202 mm mean diameter were used as fluidizing particles. Bed height at incipient fluidization was maintained at about 65 cm throughout the experiments. Main experimental conditions are shown in **Table 1**.

Bubble frequency was measured with a capacitance probe operated by 3MHz carrying wave, and was counted with a digital counter for 60 seconds. **Fig. 1(a)** is a diagram of the capacitance probe.

* Received on August 3, 1972
Presented at the 36th Annual Meeting of the Soc. of Chem. Engrs., Japan (Tokyo, April 1971)
〒061-01 札幌市東月寒41-2
北海道工業開発試験所 富田稔

A capacitance probe was also used for the measurement of volume fraction of bubbles; the signals from the probe were integrated with a digital integrator for 60 seconds. Volume fraction of bubbles was calculated from integrated values for the fluidized bed, incipiently fluidized bed and empty column.

A strain gage probe, shown in **Fig. 1(b)**, was used for the determination of upward and downward forces acting on the probe in the fluidized bed; the signals from the probe were integrated with a digital integrator for 60 seconds. The upward and downward forces were expressed as the difference between output voltage from the integrator for the fluidized bed and that for the incipiently fluidized bed.

Iron probe supporters were mounted at the top of the columns in such a way that the probes could be fixed vertically and radially at any point within the beds.

Table 1 Experimental conditions

Apparatus
- Fluidizing tower (polymethylmethacrylate)
  - inner diameter D_T=21.4, 37.8, 59.9 cm
  - height of tower=*ca.* 100 cm
  - height of settled bed=*ca.* 65 cm
- Distributor (perforated plate)
  - hole diameter=0.1 cm
  - pitch=1.5 cm
  - fraction of hole area=0.011

Particle (sand)
- size range=0.147–0.295 mm
- mean diameter $\bar{d}_p$=0.202 mm
- absolute density ρ_s=2.65 g/cm^3
- minimum fluidizing gas velocity u_{mf}=4.0 cm/sec
- void fraction at incipient fluidization ε_{mf}=0.47
- sphericity ϕ_s=0.685
- angle of repose ϕ_r=32.5 deg.

Fluid (air at 1 atm., room temperature)
- fluidizing gas velocity u_0=10, 15, 20, 25 cm/sec

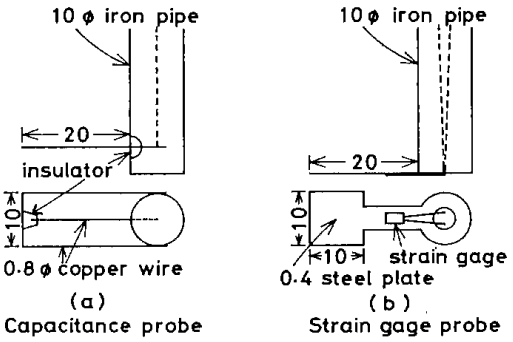

Fig. 1 Capacitance probe and strain gage probe

3. Experimental Results and Discussion

3. 1 Bubble frequency

Local bubble frequencies were measured at various levels and radial positions in each bed. Typical examples of the results are shown in **Fig. 2**. The general shape of the bubble frequency distribution was almost the same as those previously observed in cylindrical beds[5,9]. At lower levels of bed, the bubble frequency seemed to increase near the wall of the bed. At higher levels the distribution of the bubble frequency was observed to be almost uniform in each bed.

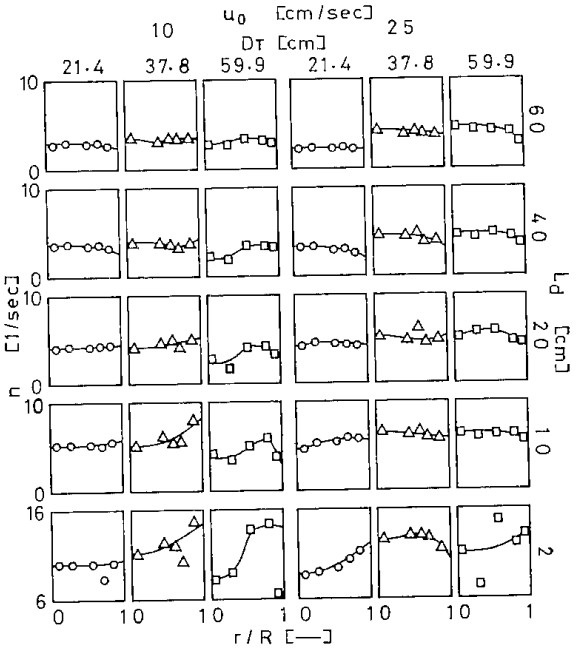

Fig. 2 Distribution of bubble frequency

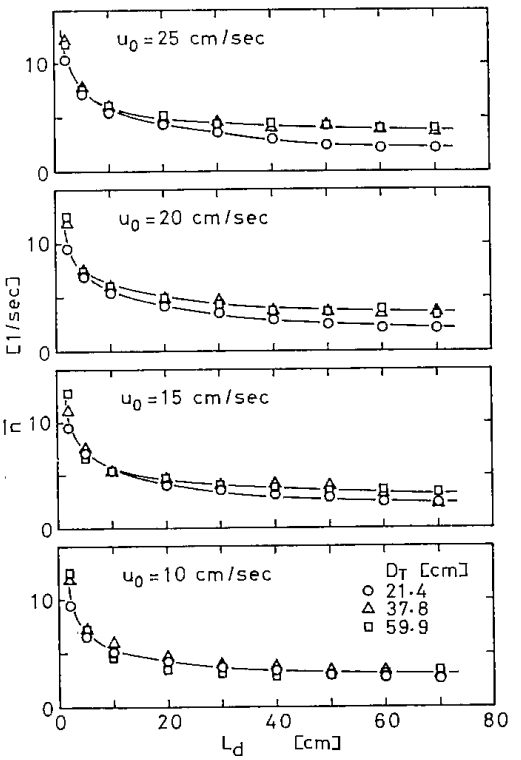

Fig. 3 Longitudinal distribution of mean bubble frequency

Fig. 3 shows the longitudinal distributions of $\bar{n}$, the bubble frequency averaged across the sectional area. In every experiment, $\bar{n}$ decreased rapidly up to a level of

about 20 cm from the distributor and then decreased slowly. At higher gas velocities, decreasing rate of $\bar{n}$ at higher levels in the bed of 21.4 cm I.D. was bigger than those in the beds of 37.8 and 59.9 cm I.D.

3. 2 Volume fraction of bubbles

Volume fraction of bubbles ε_b was measured at various levels and radial positions in each bed, and typical examples of the results regarding its distribution are shown in **Fig. 4**. The volume fraction of bubbles just above the distributor seemed to be large in the central portion as well as near the wall for the bed of 21.4 cm I.D. However, it became large near the wall for the bed of 37.8 cm I.D., and in the central portion for the bed of 59.9 cm I.D. At higher levels in the beds of 21.4 and 37.8 cm I.D., a peak of the distribution of ε_b was observed in the central portion at higher gas velocities, but not at lower gas velocities. On the other hand, at higher levels in the bed of 59.9 cm I.D., the distribution of ε_b was radially uniform at higher gas velocities, and had a tendency to produce a peak in the central portion at lower gas velocities.

Fig. 5 shows the longitudinal distributions of $\bar{\varepsilon}_b$, the volume fraction of bubbles averaged across the sectional area. At higher gas velocities $\bar{\varepsilon}_b$ was large just above the distributor, but decreased rapidly up to a level of about 10 cm from the distributor and then became almost constant at higher levels.

3. 3 Rising velocity of bubbles

By application of Kunii and Levenspiel's "bubbling bed model"[6], a material balance of gas in the section of the bed under consideration gives

$$u_0 = \bar{\varepsilon}_b u_b + \bar{\varepsilon}_b \alpha \varepsilon_{mf} u_b + \bar{\varepsilon}_b \beta \varepsilon_{mf} u_b + (1 - \bar{\varepsilon}_b - \bar{\varepsilon}_b \alpha - \bar{\varepsilon}_b \beta)\varepsilon_{mf} u_e \qquad (1)$$

where u_e is the upward velocity of gas flowing through the emulsion phase, and is given by

$$u_e = (u_{mf}/\varepsilon_{mf}) - u_s \qquad (2)$$

where u_s is the downward velocity of solid particles in the emulsion phase, and is given by

$$u_s = \bar{\varepsilon}_b \beta u_b / (1 - \bar{\varepsilon}_b - \bar{\varepsilon}_b \beta) \qquad (3)$$

By substituting Eqs.(2) and (3) into Eq.(1), the mean rising velocity of bubbles in the section of bed u_b is expressed as

$$u_b = \frac{u_0 - (1 - \bar{\varepsilon}_b - \bar{\varepsilon}_b \alpha - \bar{\varepsilon}_b \beta) u_{mf}}{\bar{\varepsilon}_b \left\{ 1 + (\alpha + \beta)\varepsilon_{mf} - \left(\frac{1 - \bar{\varepsilon}_b - \bar{\varepsilon}_b \alpha - \bar{\varepsilon}_b \beta}{1 - \bar{\varepsilon}_b - \bar{\varepsilon}_b \beta} \right) \beta \varepsilon_{mf} \right\}} \qquad (4)$$

The ratio of cloud volume in the emulsion phase to bubble volume α in Eq.(4) is defined as

$$\alpha = (V_c - V_b)/V_b \qquad (5)$$

where V_c and V_b are the volume of clouds and the volume of bubbles, respectively. The ratio V_c/V_b can be estimated by Murray's equation[8] with $\theta = \pi/2$ such as Chiba and Kobayashi[4] have adopted.

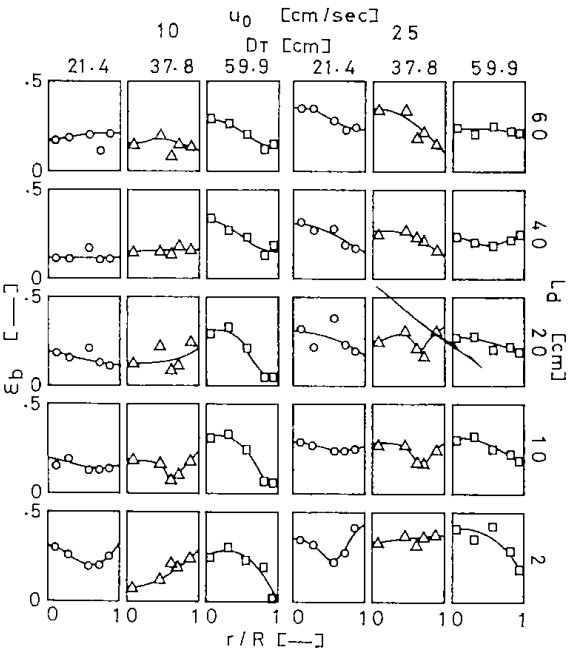

Fig. 4 Distribution of volume fraction of bubbles

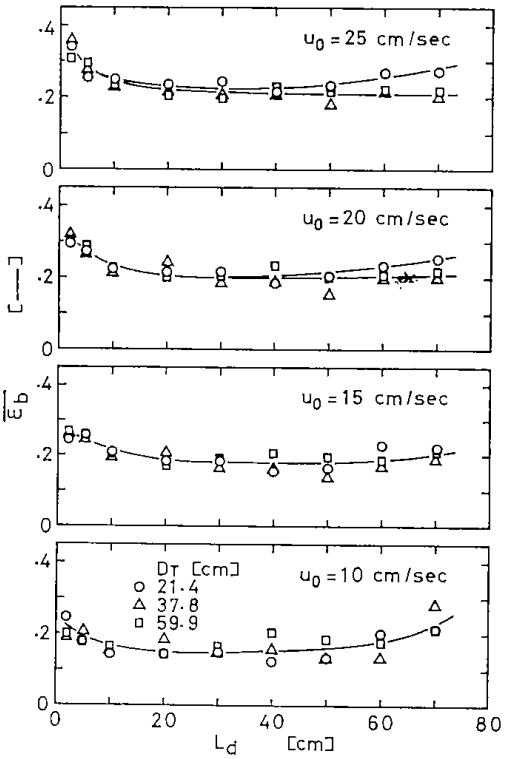

Fig. 5 Longitudinal distribution of mean volume fraction of bubbles

$$V_c/V_b = \gamma/(\gamma - 1)\text{: Murray's equation } (\theta = \pi/2) \qquad (6)$$

where

$$\gamma = (u_b + u_s)(\varepsilon_{mf}/u_{mf}) \tag{7}$$

From Eqs.(3), (5), (6) and (7), one can obtain

$$\alpha = \frac{(1 - \bar{\varepsilon}_b - \bar{\varepsilon}_b\beta)u_{mf}}{(1 - \bar{\varepsilon}_b)\varepsilon_{mf}u_b - (1 - \bar{\varepsilon}_b - \bar{\varepsilon}_b\beta)u_{mf}} \tag{8}$$

The ratio of wake volume to bubble volume β is estimated from the experiments of Rowe and Partridge[10] as β=0.22 in this paper, and it is assumed that β is constant throughout the bed.

Using a trial-and-error method, u_b can be calculated from the observed $\bar{\varepsilon}_b$ and Eqs.(4) and (8). The longitudinal distributions of u_b are shown in **Fig. 6**. The u_b increased rapidly just above the distributor and approached an almost constant value at levels higher than 10 cm from the distributor.

3. 4 Bubble diameter

According to Kunii and Levenspiel's model[6], the frequency of bubbles passing a point n' is given by

$$n' = u_b/h \tag{9}$$

where h is the height between two successive bubbles registered on the point. Assuming that the sum of a bubble's volume and its wake volume is equal to the volume of sphere with a diameter of d_b, the volume of the bubble is $\pi d_b^3/6(1+\beta)$. On the average, h is related to $\bar{\varepsilon}_b$ by

$$\bar{\varepsilon}_b = \frac{d_b^3/6(1 + \beta)}{d_b^2 h/4} \tag{10}$$

Combining Eqs.(9) and (10) and eliminating h gives

$$d_b = \frac{3(1 + \beta)\bar{\varepsilon}_b u_b}{2n'} \tag{11}$$

On the other hand, the frequency of bubbles passing the head of a probe n is related to n' by

$$n' = \left(\frac{\pi d_b^2/4}{A}\right)n \tag{12}$$

where A is the detectable area of the probe. In this paper, A is given by

$$A = (\pi d_b^2/4) + (b + l)d_b + bl \tag{13}$$

where b and l are the lengths of the short and long sides of the probe, respectively.

The mean bubble diameter in the section of given level d_b can be calculated from $\bar{\varepsilon}_b$, u_b, n, and Eqs.(11) and (12) using a trial-and-error method. The longitudinal distributions of d_b are shown in **Fig. 7**. For the beds of 37.8 and 59.9 cm I.D., d_b increased rapidly up to a level 20 cm from the distributor, and then slowly at levels higher than 30 cm. However, for the bed of 21.4 cm I.D. at higher gas velocities, d_b increased approximately in proportion to levels even at levels higher than 30 cm from the distributor. Therefore, it is considered that the behavior of bubbles is strongly affected by the wall of the bed as the bubbles grow relatively large compared with the bed diameter. The diameter and rising velocity of bubbles evaluated in

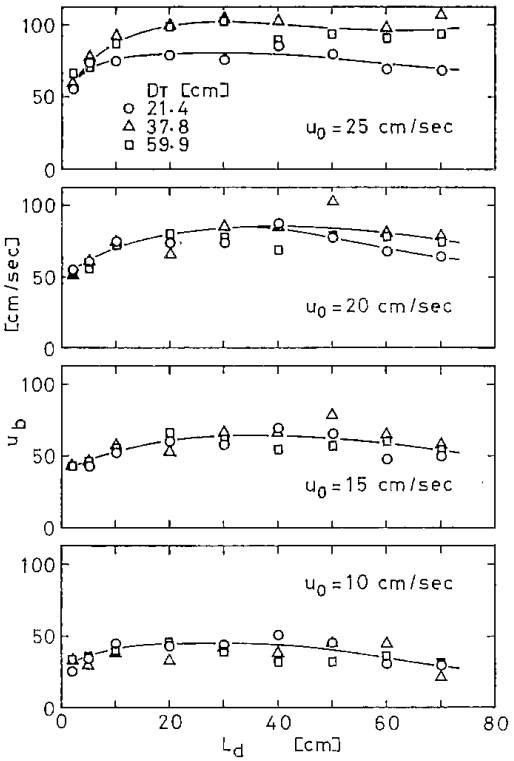

Fig. 6 Longitudinal distribution of mean bubble rising velocity, calculated by Eqs.(4) and (8)

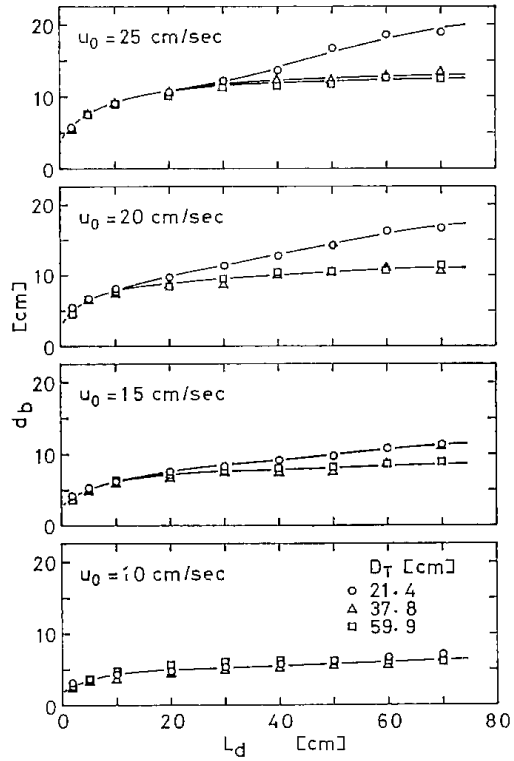

Fig. 7 Longitudinal distribution of mean bubble diameter, calculated by Eqs.(11) and (12)

this way are only approximate, but may be valuable as parameters for semi-quantitative analysis.

3. 5 Relationship between bubble diameter and rising velocity

Fig. 8 shows the relationship between the bubble diameter and rising velocity evaluated. In the region up to 20 cm from the distributor, the rising velocity of bubbles seemed to be approximately proportional to $d_b^{0.8}$ in each bed. At higher levels than 30 cm from the distributor in the beds of 37.8 and 59.9 cm I.D., the rising velocity of bubbles was approximately proportional to $d_b^{1.2}$. At the higher levels in the bed of 21.4 cm I.D., the rising velocity of bubbles was relatively lower than in the beds of 37.8 and 59.9 cm I.D. The lower rising velocity of bubbles in the bed of 21.4 cm I.D. suggests that this bed is in a slug flow condition at higher gas velocities.

3. 6 Upward and downward forces

Upward and downward forces acting on the probe in fluidized bed F_s were measured at various levels and radial positions in each bed, and typical examples of their distribution are shown in **Fig. 9**, where a positive value of F_s corresponds to upward force and a negative value to downward force. The distribution curve of F_s had a peak near the wall of the bed just above the distributor, and the peak moved towards the central portion with increase of level. This tendency was significant when gas velocity and bed diameter were increased. Furthermore, for the bed of 59.9 cm I.D. at higher gas velocities, two peaks were found in the distribution curve of F_s at higher levels.

Assuming that F_s is proportional to the bulk flow rate of the particles, the flow pattern of the particles throughout the bed is estimated from the distribution of F_s as follows. In the region of lower levels up to 30–40 cm from the distributor, there was a bulk circulation where the particles flowed up along the wall of the bed and flowed down through the central portion in the bed. At levels higher than 30–40 cm from the distributor, there was another bulk circulation where the particles flowed down along the wall of the bed and flowed up through its central portion. In particular, for the bed of 59.9 cm I.D., the several bulk circulations seemed to take place in the region of higher levels at higher gas velocities, as predicted by Kunii *et al.*[5,6].

4. Conclusion

The bubble frequency, volume fraction of bubbles, and upward and downward forces were measured in fluidized beds of 21.4, 37.8 and 59.9 cm I.D. Sands of 0.202 mm mean diameter were fluidized by air with superficial velocity ranging up to 25 cm/sec. The measurements were carried out with a capacitance probe and a strain gage probe. The diameter and rising velocity of bubbles were evaluated by analyzing the experimental data on the basis of the bubbling bed model proposed by Kunii and Levenspiel. The effect

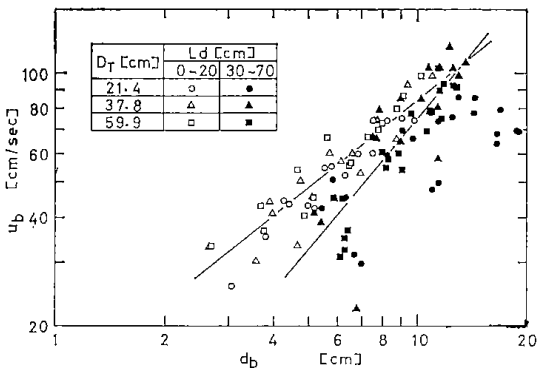

Fig. 8 Relationship between bubble diameter and bubble rising velocity

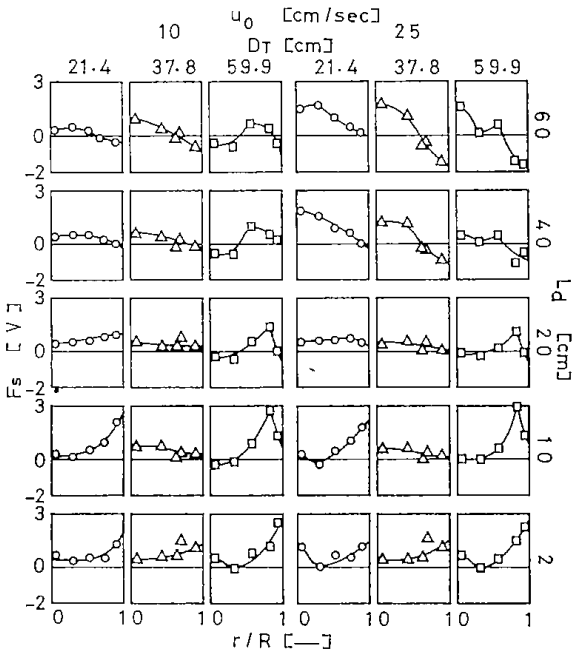

Fig. 9 Distribution of upward and downward forces

of bed diameter on the behavior of bubbles and the flow pattern of particles in the fluidized beds were discussed, using the experimental and evaluated results.

To summarize:

1) In the lower level region of the bed, up to about 20 cm from the distributor, small bubbles formed just above the distributor coalesced, grew rapidly and tended to crowd in the central portion in the bed. The rising velocity of bubbles was approximately proportional to the 0.8 power of bubble diameter.

2) In the higher level region of the bed, above 20 cm or thereabout, the bubbles in a small-scale bed coalesced more and the bed reached a slug flow condition. The rising velocity of bubbles was relatively lower than in a large-scale bed. On the other hand, the bubbles in a large-scale bed coalesced somewhat and flowed up steadily through the central portion in the bed. The rising velocity of bubbles was approximately proportional to the 1.2 power of bubble diameter.

3) In the lower level region of the bed, there was a bulk circulation of the particles, which flowed up along the wall of the bed and flowed down through the central portion in the bed. In the higher level region of the bed, there was another bulk circulation of the particles, which flowed down along the wall of the bed and flowed up through its central portion. In particular, in the higher level region of a large-scale fluidized bed the several bulk circulations of the particles seemed to take place at higher fluidizing gas velocities.

Nomenclature

A	= detectable area of a probe	[cm^2]
b	= length of short side of a probe	[cm]
d_b	= bubble diameter	[cm]
$\bar{d}_p$	= mean particle diameter	[mm]
D_T	= bed diameter	[cm]
F_s	= output voltage from an integrator corresponding to upward and downward forces acting on a probe in fluidized bed	[volt]
h	= height between two successive bubbles registered on a probe	[cm]
l	= length of long side of a probe	[cm]
L_d	= bed level from distributor	[cm]
n	= frequency of bubbles passing the head of a probe	[1/sec]
n'	= frequency of bubbles passing a point	[1/sec]
$\bar{n}$	= mean bubble frequency	[1/sec]
r	= distance from the center of a column	[cm]
R	= radius of a column	[cm]
u_b	= velocity of bubble rising through a bed	[cm/sec]
u_e	= upward velocity of gas through the emulsion phase	[cm/sec]
u_{mf}	= superficial velocity of fluidizing gas (based on empty column) at incipient fluidization	[cm/sec]
u_0	= superficial velocity of fluidizing gas based on empty column	[cm/sec]
u_s	= mean downward velocity of solid particles in the emulsion phase	[cm/sec]
V_b	= volume of bubble	[cm^3]
V_c	= volume of gas cloud	[cm^3]
α	= ratio of cloud volume to bubble volume	[−]
β	= ratio of wake volume to bubble volume	[−]
γ	= defined in Eq.(7)	[−]
ε_b	= volume fraction of bubbles	[−]
$\bar{\varepsilon}_b$	= mean volume fraction of bubbles	[−]
ε_{mf}	= void fraction at incipient fluidization	[−]
θ	= angle	[degrees]
π	= ratio of circumference to diameter	[−]
ρ_s	= absolute density of solid particle	[g/cm^3]
ϕ_r	= angle of repose	[degrees]
ϕ_s	= sphericity of a particle	[−]

Literature Cited

1) de Groot, J. H.: "Proceedings of the International Symposium on Fluidization", p.348, Netherlands University Press, Amsterdam (1967)
2) Hovmand, S., W. Freedman and J. F. Davidson: *Trans. Instn. Chem. Engrs.* (London), **49**, 149 (1971)
3) Ikeda, Y.: *Kagaku Kōgaku*, **34**, 1013 (1970)
4) Kobayashi, H., F. Arai, T. Chiba and Y. Tanaka: *Kagaku Kōgaku*, **33**, 274 (1969)
5) Kunii, D., K. Yoshida and I. Hiraki: "Proceedings of the International Symposium on Fluidization", p. 243, Netherlands University Press, Amsterdam (1967)
6) Kunii, D. and O. Levenspiel: "Fluidization Engineering", John Wiley and Sons, Inc., New York (1969)
7) May, W. G.: *Chem. Eng. Progr.*, **55**, 49 (1959) and **56**, 43 (1960)
8) Murray, J. D.: *J. Fluid Mech.*, **22**, (Part 1), 57 (1965)
9) Park, W. H., W. K. Kang, C. E. Capes and G. L. Osberg: *Chem. Eng. Sci.*, **24**, 851 (1969)
10) Rowe, P. N. and B. A. Partridge: *Trans. Instn. Chem. Engrs.* (London), **43**, T157 (1965)
11) Whitehead, A. B. and A. D. Young: "Proceedings of the International Symposium on Fluidization", p. 284 and 294, Netherlands University Press, Amsterdam (1967)

(Journal of Chemical Engineering of Japan, vol.6, No.2 (1973) Pages 196~201.)

Infrared Studies on Water Adsorption Systems with the Use of HDO. I. Molecular Sieves 13X and 4A

Masao HINO

Government Industrial Development Laboratory, Hokkaido, Higashi-Tsukisamu, Toyohira-ku, Sapporo 061-01

(Received July 12, 1976)

It was shown that the use of HDO molecules in IR studies on water adsorption system is advantageous for obtaining information as to whether 1) a band arises from the surface structural hydroxyl groups or from adsorbed water molecules, 2) a band arises from an overtone bending vibration, and 3) water molecules are adsorbed in a state of its two hydroxyl bonds being equivalent. The bands in the spectra of Molecular sieves–H_2O systems were assigned as follows. I) 13X–H_2O system. Bands at 3752, 3685, and 3647 cm^{-1} correspond to surface structural OH, bands at 3697, 3360, and 1650 cm^{-1} to asymmetrically adsorbed water molecules, band at 3230 cm^{-1} to overtone bending vibration of the same molecules. The band at 3590 cm^{-1} was found to arise from some other type of adsorbed water molecules. II) 4A–H_2O system. Bands at 3500, 3400, and 1660 cm^{-1} correspond to symmetrically adsorbed water molecules, band at 3280 cm^{-1} to overtone bending vibration of the same molecules. Another type of adsorbed water was suggested to be present.

Infrared spectroscopy has been widely employed in studies on surface and adsorbed species. However, analysis of the spectra has not always been easy to carry out. This is due to inevitable characteristics of the spectra of adsorption systems, such as the specific complexity of the spectra and the lack of means of spectral observation over a wide frequency range masked by strong absorption by adsorbents.

Thus, additional information from other sources is desirable. As an example, the use of partially deuterated compounds is considered to be effective. The use of this technique has been made for the spectral study on adsorption systems to some extent.[1] A number of investigations have been carried out on water adsorption systems. However, they were restricted to the measurement of the spectra of H_2O or D_2O adsorption systems. No work seems to have been made with the use of HDO.

In the present work, IR absorption spectra of hydroxyls and adsorbed water on Molecular sieves 13X and 4A are analyzed by the use of HDO. Although assignments of the spectral bands of these systems have been made to a certain extent,[2-14] more direct and conclusive evidences for the assignments are obtained by the use of the present technique.

Its applicability to other molecular adsorption systems will be suggested.

Experimental

Materials. Linde molecular sieves 13X and 4A (GASUKURO Ind. Co., Ltd.) were used. The crystallinity and purity of these materials were confirmed to be of a sufficiently high by X-ray diffraction analysis. The surface area of the 13X sieve was 717 m^2/g. In order to obtain extremely fine powder samples for IR experiments, the materials were ground in an agate motor with a small amount of water, and then suspended in deionized water. The particle size of the fine powders was found to be less than 1μm in diameter by electron microscopic observation. D_2O (E. Merck, Darmstadt) of 99.75% in purity and deionized-distilled H_2O were used for IR experiments after being degassed.

Apparatus and Procedure. A JASCO Model 402-G IR spectrophotometer and a Pyrex glass cell were used for recording the spectra. The cell was essentially similar to that designed by Angell *et al.*[6] In order to prevent the contamination of the sample pieces by grease vapor, a Teflon greaseless valve was fixed directly to the top of the cell. The exchange of sample pieces was made by cutting and re-fixing the arm part of the cell.

The sample powders were pressed into disks under a pressure of 2.5 tons/cm^2, and then the disks were cut into pieces of 1×2 to 2.5 cm to fit the cell windows. The "thickness" was 12—80 mg/cm^2.

After the sample pieces had been set in the cell, they were evacuated at 500 °C for at least 3 h prior to experiments. Before the addition of each type of sample water for IR measurements, the surface of the sample as well as the inner wall of the cell were washed by the following procedure. The sample was exposed at room temperature to the saturated sample water vapor, and then pumped out at 180—200 °C for 10 min. This procedure was repeated five times. Finally, it was evacuated at 500 °C for 3 h. Spectral observation confirmed that the washing was sufficient. In the case of measurements of H_2O-adsorbent systems on a new sample piece, washing was omitted.

The experiments related to HDO were carried out in the presence of H_2O and D_2O. By mixing H_2O with D_2O at a molar ratio of a to b, HDO is obtained under the coexistence of other water in a ratio of about H_2O: HDO: $D_2O = a^2 : 2ab : b^2$.

All the spectra were measured at room temperature. Spectra on the desorption process were observed after the pretreated sample piece was first exposed to the saturated sample water vapor and then evacuated at various temperatures. Spectra on the adsorption process were measured by dosing small amounts of sample water at room temperature successively after the sample piece was evacuated at 500 °C.

The measurements were carried out mainly in the OD stretching region in place of the OH stretching region, since the former is not only higher in transparency but also flatter in background owing to the lack of weak absorption bands arising from the water vapor in the air.

Results

13X–Water System. D_2O, H_2O Systems: The spectra of 13X–D_2O and H_2O systems were measured for a comparison of the results with those of the HDO system (Figs. 1 and 2). The spectra observed were similar to those published.[17] On evacuation at 90 °C six absorption bands were observed at 2756, 2727, 2682, 2645, 2470, and 2395 cm^{-1} in the D_2O system, (these

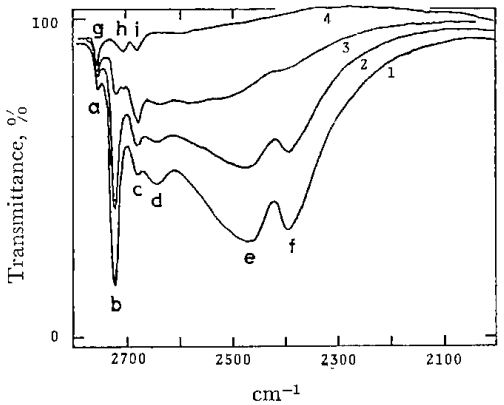

Fig. 1. Spectra of 13 X–D_2O system.
Evacuated for (1) 1 h at 90 °C, (2) 1 h at 120 °C, (3) 20 min at 170 °C, (4) 2 h at 500 °C. "Thickness" of the sample piece was 12 mg/cm².

bands as well as the corresponding bands in other systems will be referred to as a, b, c, d, e, and f). In the H_2O system the six bands corresponding to those in D_2O system were at 3752, 3697, 3645, 3590, *ca.* 3360, and 3230 cm^{-1}. In the latter system a single HOH bending vibration band was observed at 1650 cm^{-1}. Elevation of the evacuation temperature gave rise to a decrease in the intensity of all these bands except for a and c. After the final evacuation at 500 °C, three sharp bands remained at 2756, 2708, and 2683 cm^{-1} in the D_2O system (referred to as g, h, and i, respectively), and in the H_2O system at 3752, 3685, 3647 cm^{-1}.

HDO System: The spectra in OD stretching and bending regions are shown in Fig. 3. In this experiment, an H_2O–D_2O mixture in the ratio 3 to 1 was used except for curve 5, the contents being H_2O 56.3%, HDO 37.5% and D_2O 6.3%. In the number of OD chemical bond, the 75% belongs to HDO and the rest to D_2O. The OH stretching region of this system (Fig. 4) was measured employing another mixture in the ratio H_2O : D_2O = 1 : 5. The spectra of OD and OH stretching regions of this system were compared with those of D_2O and H_2O systems, respectively. All the correlations

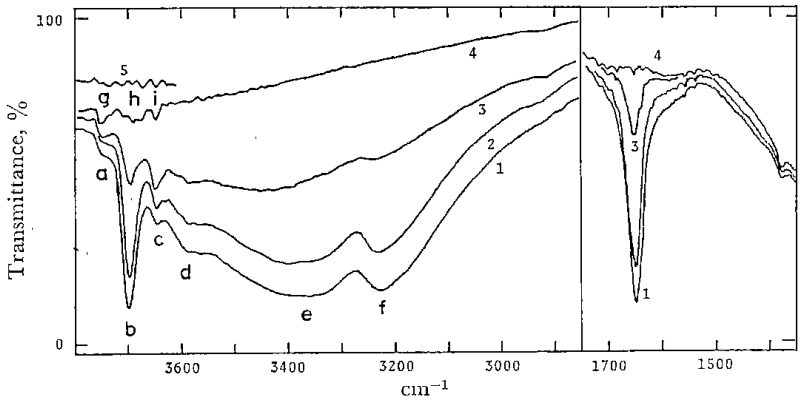

Fig. 2. Spectra of 13X–H_2O system.
Evacuated for (1) 1 h at 100 °C, (2) 1 h at 120 °C, (3) 25 min at 165 °C, (4) 2 h at 500 °C. (5) Empty cell.[16] Sample piece "thickness" 12 mg/cm².

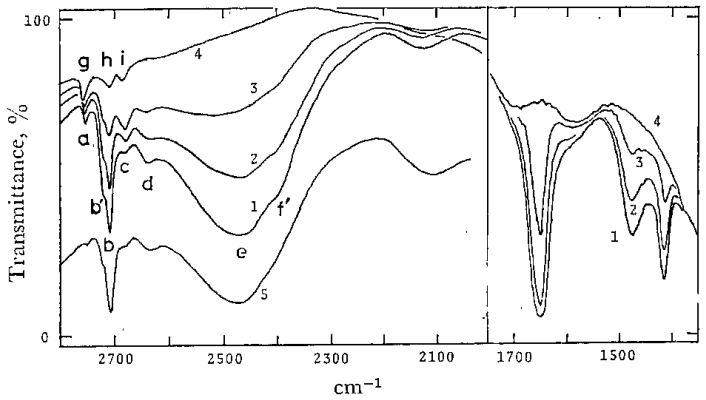

Fig. 3. Spectra of 13X–HDO system in the OD stretching and bending regions.
Evacuated for (1) 1 h at 95 °C, (2) 1 h at 120 °C, (3) 20 min at 165 °C, (4) 2 h at 500 °C after exposure to the vapor of H_2O–D_2O mixture of a molar ratio of 3 to 1, and (5) evacuated for 1 h at 90 °C after exposure to the vapor of H_2O–D_2O 7 to 1 mixture. Sample piece "thickness" 43 mg/cm².

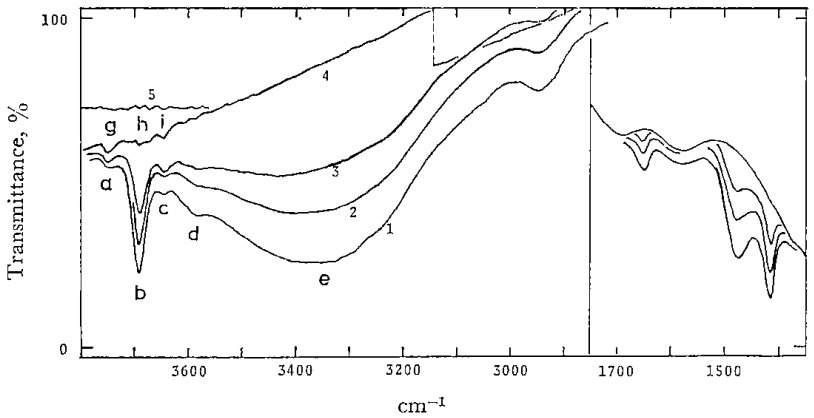

Fig. 4. Spectra of 13X–HDO system in the OH stretching and bending regions. Evacuated for (1) 1 h at 95 °C, (2) 1 h at 120 °C, (3) 20 min at 165 °C, (4) 3 h at 500 °C after exposure to the vapor of H_2O–D_2O 1 to 5 mixture. (5) Empty cell. Sample piece "thickness" 38 mg/cm².

between the spectra in the OH stretching region of HDO system and those of H_2O system were analogous to those between the spectra in the OD stretching region of the HDO system and those of D_2O system. The frequencies of the bands in OH stretching regions are parenthesized.

Bands a, c, and e in the spectra of HDO system appeared in the OD stretching region at 2756, 2680, and 2470 cm^{-1} (3750, 3645, *ca.* 3350 cm^{-1}) which were of nearly the same frequencies as those of the D_2O system. However, band b was observed at a distinctly different frequency from that of D_2O system, namely at 2710 cm^{-1} (3690 cm^{-1}). As for band d, even though the difference in frequency was not very great, *ca.* 7 cm^{-1}, the frequency 2638 cm^{-1} was not equal to that of the band in D_2O system. In the OH region, band d was so broad that the difference could not be detected decisively. It should be noted that no band f appeared in the spectra of this system. The fact that the shoulders at 2725 and 2395 cm^{-1} are due to the D_2O molecules contained in the mixed water as "impurity" was confirmed from another experiment, *viz.* the spectra after the adsorption of sample water followed by evacuation at 100 °C were measured in a series where the D content of the sample water was changed step by step from 0 to 100 atom %. The results showed that the intensities of both shoulders change in proportion to the D content. The spectrum in the OD stretching region obtained by the use of H_2O: D_2O=7.1: 1.0 mixed water is shown in Fig. 3, curve 5. A band somewhat broader and weaker appeared in both stretching regions, at 2945 cm^{-1} in the OH region and at 2120 cm^{-1} in the OD region. The weak absorption bands of g, h, and i were measured in the OD stretching region with a thick sample for the sake of comparison with those in D_2O system. The results showed that the three bands were exactly equal in wavenumber to those in D_2O system, and were 27% in intensity as compared with that of the latter which is almost equal to the D content, 25 atom %, of the mixed water used. In the bending vibration region, three absorption bands were observed at 1650, 1476, and 1415 cm^{-1}. The band at 1650 cm^{-1} is assigned to HOH bending vibration, because its frequency was quite the same as that of pure H_2O system and its intensity decreased with decrease of H_2O content in the mixed water (Figs. 3 and 4). Thus the other two arise from HDO.

The spectra measured on the adsorption process were almost the same as those on the desorption process. However, the intensity of the band d was so weak that the band was hardly observable on the adsorption process in the spectra of any of the systems.

4A–Water System. In this system the spectral measurements were carried out only on the adsorption process.

4A–D_2O, H_2O Systems: In the stretching region of the spectra of D_2O (H_2O) system (Figs. 5 and 6) three main bands were observed at 2578, 2515, and 2427 cm^{-1} (in H_2O system, at 3500, 3400, and 3280 cm^{-1}) and three weak bands at 2760, 2737, and 2645 cm^{-1} (in H_2O system, only the two former bands were detected at 3750 and 3715 cm^{-1}). In H_2O system one bending band was observed at 1660 cm^{-1}. These were similar to those reported by previous authors.[7,8]

4A–HDO System: The spectra obtained in the OD stretching and bending regions employing an H_2O–D_2O

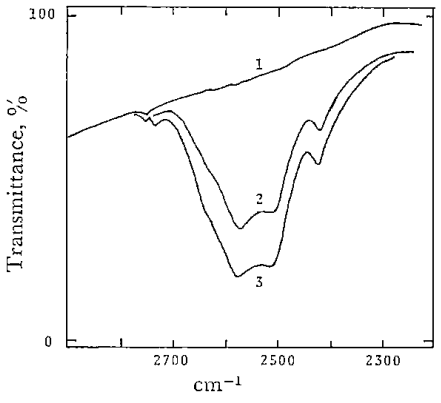

Fig. 5. Spectra of 4A–D_2O system.
(1) Evacuated for 3 h at 500 °C, (2) 9 μmol, (3) 18 μmol of D_2O readsorbed. Sample piece "thickness" 30 mg/cm².

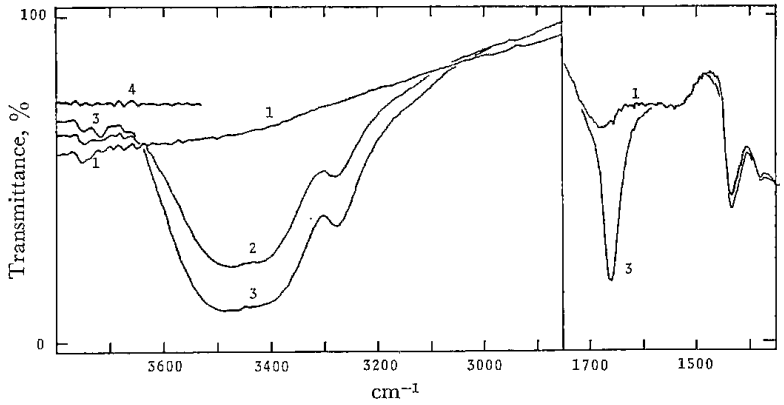

Fig. 6. Spectra of 4A–H_2O system.
(1) Evacuated for 3 h at 500 °C, (2) 9μmol, (3) 18 μmol of H_2O readsorbed.
(4) Empty cell. Sample piece "thickness" 15 mg/cm².

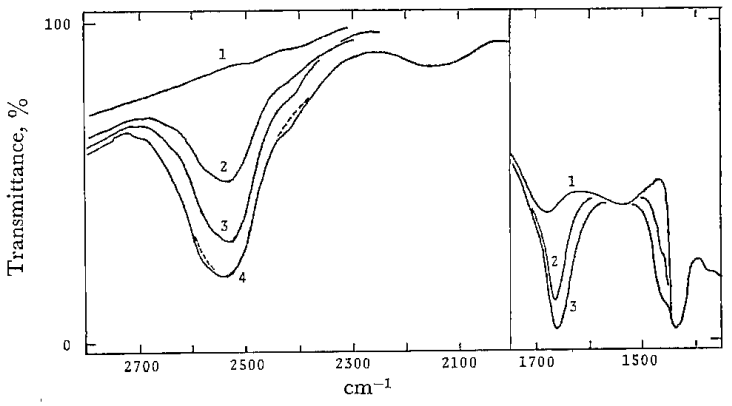

Fig. 7. Spectra of 4A–HDO system in the OD stretching and bending regions.
(1) Evacuated for 3 h at 500 °C, (2) 18 μmol, (3) 36 μmol, (4) 54 μmol of H_2O–D_2O 3 to 1 mixture were readsorbed. Sample piece "thickness" 30 mg/cm².

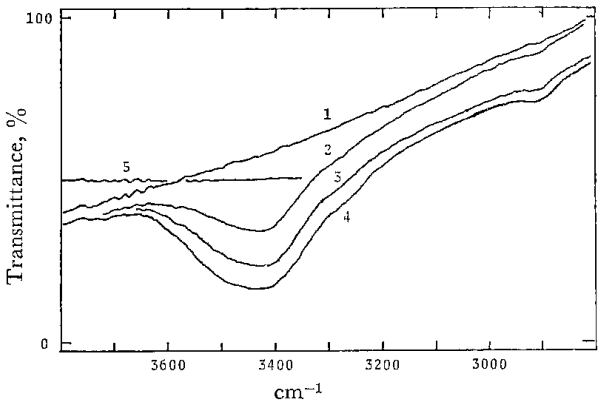

Fig. 8. Spectra of 4A–HDO system in the OH stretching region.
(1) Evacuated for 3 h at 500°C, (2) 18 μmol, (3) 36 μmol, (4) 54 μmol of H_2O–D_2O 1 to 5 mixture were readsorbed. (5) Empty cell. Sample piece "thickness" 30 mg/cm².

mixture in the ratio 3 to 1 and those in the OH stretching region employing another mixture in the ratio 1 to 5 are shown in Figs. 7 and 8, respectively. In each stretching region, a main single OD or OH stretching band of symmetric shape appeared at a frequency of 2530 or 3420 cm^{-1}. Their positions are located between two strong stretching bands appearing in the spectra of D_2O or H_2O system. A weak band was observed at 2705 cm^{-1} in the OD stretching region but not the fitting band in the OH region. As in the case of 13X–water system a new band was observed in each stretching region at 2140 cm^{-1} in the OD region and at 2910 cm^{-1} in OH region. Both bands at 2427 cm^{-1} in D_2O system and 3280 cm^{-1} in H_2O system disappeared from each corresponding region of the spectra of HDO system. Swellings around 2580, 2420 cm^{-1} (Fig. 7) and 3500, 3280 cm^{-1} (Fig. 8) arise obviously from D_2O or H_2O present in the water mixtures. Only one HOD bending band appeared at 1465 cm^{-1}. The 1660 cm^{-1} band corresponds to HOH bending vibration as previously described.

Table 1. Summary of the IR bands of molecular sieves–water systems

Band sign	D_2O system (cm^{-1})	H_2O system (cm^{-1})	HDO s-stem (cm^{-1}) Stretching regions OD	Stretching regions OH	Bending region	Assign
			[13X-water System]			
a (g)	2756	3752	2756	3750		1)
b	2727	3697	2710	3690		2)
c (i)	2682	3645	2680	3645		3)
d	2645	3590	2638	3590		4)
e	2470	3360	2470	3350		5)
f	2395	3230				6)
h	2708	3685	2708	3685		7)
				2945		8)
		2120				9)
		1650			1476, 1415	10)
b′			(2725)		(1650)	11)
f′			(2395)			11)
			(2120)			11)
			[4A-water System]			
	2760	3750				12)
	2737	3715	2705			13)
	2645					13)
	2578	3500	2530	3420		14)
	2515	3400				14)
	2427	3280				15)
				2910		16)
		1660			1465	17)
			(2580)	(3500)	(1660)	18)
			(2420)	(3280)		18)
			(2140)			18)

1), 3), 7), 12) OD(H) stretching of structural deuteroxyl groups. 2), 5), 10) Free OD(H) stretching, hydrogen-bonded OD(H) stretching and HOH (HOD) bending of asymmetrically adsorbed water (Type WX–I), respectively. 4), 13) OD(H) stretching of adsorbed water of Types WX–II and WA–II, respectively. 6), 15) DOD(HOH) overtone bending of Types WX–I and WA–I water, respectively. 8), 16) HOD overtone bending or combination of adsorbed HDO? 9) Combination of adsorbed H_2O. 11), 18) Arising from D_2O or H_2O impurities. 14) OD (H) stretching of symmetrically adsorbed water (Type WA–I). 17) HOH(HOD) bending of Type WA–I water.

The observed bands are summarized with their assignments in Table 1.

Discussion

13X–Water System. Discussion has been made as to whether various absorption bands, especially those of h, i, d, and b, arise from surface hydroxyl groups or from adsorbed water molecules.[15] The use of HDO gives more detailed information. If a band arises from the former, the wavenumbers of the corresponding two OH (or OD) vibration bands, one appearing in the H_2O (or D_2O) adsorption system and the other in the HDO adsorption system, should be exactly the same as each other, and if it arises from the latter the wave numbers would not be equal. Thus, the residual bands g, h, and i can be attributed to the stretching vibrations of surface hydroxyl groups, since their corresponding bands appear at the same frequency in the two systems. Bands a and c are also attributable to hydroxyl groups. They would be the same bands as g and i, respectively, because of equal frequency. However, the origin of band b differs from that of h. The fact that band b in HDO system appears in the OD stretching region at a frequency 16 cm^{-1} lower than that in D_2O system (as well as in the OH stretching region 7 cm^{-1} lower than that in H_2O system) indicates that the band does not arise from structural hydroxyl groups but from adsorbed water molecule. Band e is attributed to the OH stretching vibration of the water molecules hydrogen bonded to the surface. The absorption d was reported by Habgood,[5] Ward[9] and also by Kiselev *et al.*[12] However, no assignment was made. Only Uytterhoeven *et al.*[11] attributed the band to OH groups in ions of the type $Me^+(OH)$. However, the results in the present experiments indicate that its origin is not the structural OH groups but a certain type of adsorbed water molecule. Band f was considered by Ward[9] and Abramov *et al.*[14] to arise from the OH stretching of another type of water molecule adsorbed in a different way from the origin of band e. Kiselev *et al.*[12] attributed it to the overtone bending vibration of the water molecules, which are the origin of band e, enhanced by Fermi resonance. Our results support the assignment by Kiselev *et al.* The frequencies of the overtone bending vibrations of HDO would be near 2952 and 2830 cm^{-1} if they appear, since the fundamentals were observed at 1476 and 1415 cm^{-1}. However, since they differ a great deal from the frequency of any stretching vibration of HDO, no resonance would occur. Thus, if the band arises from the overtone bending vibration it would not appear in the spectra of HDO system, or would be only slightly observable at frequencies near 2952 and 2830 cm^{-1}. There is some uncertainty in the attribution of the observed 2945 cm^{-1} band to the overtone bending of HDO molecules. If we suppose that the 2945 cm^{-1} band is the overtone of 1476 cm^{-1} band, we cannot explain the reason why that of 1415 cm^{-1} band does not appear. However, at least the disappearance of band f from the spectra of HDO system is in line with the assignment by Kiselev *et al.* On the other hand, if Ward's assignment is accepted, no reason can be found for the disappearance of the band.

There were two bending vibrations in the adsorbed HDO molecules, but only one in adsorbed H_2O. This supports the schematic structure of water adsorption originally proposed by Bertsch and Habgood[3] (I). If the structure is adopted, the adsorbed HDO molecules would take either of the two forms onto the surface by equal chance as illustrated in (II)-a and (II)-b, then the adsorbed HDO molecules as well as the H_2O

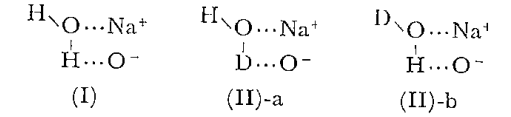

molecules should yield the bending vibrations in accordance with the observed results. This adsorption model also supports the experimental fact on the stretching vibration of the adsorbed molecules. There were two OH (OD) stretching vibration bands, one of free OH (OD, band b) and the other of hydrogen bonded OH (OD, band c), in both spectra of H_2O (D_2O) and HDO systems.

4A–Water System. First, the band at 3280 cm^{-1} in the spectra of H_2O system (at 2427 cm^{-1} in the D_2O system) is assigned to the overtone bending of adsorbed H_2O (D_2O) in the same manner as in the discussion on 13X–water system, although there remains some doubt in attributing the 2910 cm^{-1} band in HDO system to the overtone of 1465 cm^{-1} band in analogy of the case of 13X–water system. Then, the existence of two strong OH (OD) stretching bands, presumably corresponding to the ν_3 and ν_1 vibrations, and one bending band in the spectra of H_2O (D_2O) system suggests that there exists only one adsorbed species with two equivalent hydroxyl bonds. This is also supported by HDO adsorption experiment. If HDO molecule is adsorbed in this manner, OH, OD stretching bands and HOD bending band arising from the adsorbed molecule should all be single. This is in line with the observed results.

The weak bands at 2737 and 2645 cm^{-1} (Fig. 5) are possibly assigned to the ν_3 and ν_1 vibrations of another adsorbed D_2O molecule, which may fit the origin of the weak 2705 cm^{-1} band in HDO system (Fig. 7). However, the reason is not clear why the bands corresponding to them, except for at 3715 cm^{-1} in H_2O system, do not appear in the OH regions.

Bands at 2945, 2120 cm^{-1} in 13X–HDO System and at 2910, 2140 cm^{-1} in 4A–HDO System. The frequency ratios of each couple of bands, 1.39 and 1.36, seem to suggest that they arise from OH and OD stretching vibrations of HDO molecules adsorbed. However, these assignments contradict the fact that the frequencies are too low and no band corresponding to them could be detected in the spectra of H_2O or D_2O adsorption systems. In order to investigate the origin of these bands the spectra of pure H_2O, D_2O and mixtures of D_2O and H_2O were measured in liquid phase. The results show that there is a band at 2140 cm^{-1} in the spectrum of pure H_2O, its intensity decreasing with a decrease in H_2O content. No band around 2945—2910 cm^{-1} was detected in the spectrum of either pure H_2O or D_2O, but a band appeared in the spectra of mixed waters at 2920 cm^{-1}. Simultaneously, an HOD bending band was observed at 1450 cm^{-1} in the latter spectra. From a comparison of the spectra of liquid water with those of adsorption systems, the band at 2120 or 2140 cm^{-1} is considered to arise from a combination band of adsorbed H_2O molecules existing in the mixed water. The band at 2945 or 2910 cm^{-1} can be attributed to a overtone bending or a combination band of adsorbed HDO molecule.

The present technique is widely applicable to spectral analyses of adsorption systems including XH_n type molecules, with the use of partially deuterated $XH_{n-1}D$ or XHD_{n-1} molecules. It is applicable, in some cases, to the compounds including the atomic groups of $-XH_n$ type.

The author thanks Dr. Toshio Sato for his helpful advice and Mr. Okio Nishimura for his assistance in electron microscopic techniques.

References

1) For example: T. Nakata and S. Matsushita, *J. Phys. Chem.*, **72**, 458 (1968); R. J. Kokes, *Acc. Chem. Res.*, **6**, 226 (1973); B. A. Morrow, *J. Chem. Soc., Faraday Trans. 1*, **70**, 1527 (1974).
2) H. A. Szymanski, D. N. Stamires, and G. R. Lynch, *J. Opt. Soc. Am.*, **50**, 1323 (1960).
3) L. Bertsch and H. W. Habgood, *J. Phys. Chem.*, **67**, 1621 (1963).
4) L. Carter, P. J. Lucchesi, and D. J. Yates, *J. Phys. Chem.*, **68**, 1385 (1964).
5) H. W. Habgood, *J. Phys. Chem.*, **69**, 1764 (1965).
6) C. L. Angell and P. C. Schaffer, *J. Phys. Chem.*, **69**, 3463 (1965).
7) S. P. Zhdanov, A. V. Kiselev, V. I. Lygin, M. E. Ovsepyan, and T. I. Titova, *Zh. Fiz. Khim.*, **39**, 2554 (1965).
8) L. H. Little, A. V. Kiselev, and V. I. Lygin, "Infrared Spectra of Adsorbed Species," Academic Press, London & New York (1966), Chap. 14.
9) J. W. Ward, *J. Phys. Chem.*, **72**, 4211 (1968).
10) J. W. Ward, *J. Catal.*, **11**, 238 (1968).
11) J. B. Uytterhoeven, R. Schoonheydt, B. V. Liengme, and W. K. Hall, *J. Catal.*, **13**, 425 (1969).
12) A. V. Kiselev, V. I. Lygin, and R. V. Starodubceva, *J. Chem. Soc., Faraday Trans. 1*, **68**, 1793 (1972).
13) G. Senkyr and H. Noller, *J. Chem. Soc., Faraday Trans. 1*, **71**, 997 (1975).
14) V. N. Abramov, A. V. Kiselev, and V. I. Lygin, *Zh. Fiz. Khim.*, **39**, 123 (1965).
15) Refs. 3—6, 9, 10, 12.
16) The spectrum of the empty cell was measured in order to obtain an accurate background curve including many weak absorptions arising from the water vapor in the air. The background (curve 5) was substructed from the curve 4 for the sake of obtaining net spectrum.
17) Refs. 4, 5, 8, 9, 13.

(Bulletin of the Chemical Society of Japan vol.50, No. 3, March 1977 Poges 574~579.)

HDOによる水吸着系の赤外研究

Ⅲ. Zn-Y型ゼオライト[1]

日野雅夫*・平間康子*

1. 緒　言

前報[2,3]において著者らは，赤外吸収スペクトル法による固体表面と水の吸着系の化学種の同定に，水の同位体HDOを用いることが非常に有効であることを示し，この方法を用いて，モレキュラーシーブ13X（Na-X型ゼオライト），4A（Na-A型ゼオライト）[2]およびNa-Y型ゼオライト[3]の水吸着系の解析を行った．本報では前報と同じ手法を用いて，亜鉛置換Y型ゼオライトと水の吸着系について解析を行う．

Na-Y型ゼオライト（以下，単にNa-Yなどと記す）のNaイオンを多価金属カチオンで交換すると，異性化，クラッキングその他の触媒活性が増大することは良く知られている．この活性の増大は，多価金属カチオンの強い静電場力あるいは，微量の水の存在が活性を著しく高める例が見られるところから，この静電場と水の相互作用による固体酸の形成によると考えられている．このような触媒活性の究明という観点からゼオライトと水の吸着系に関する研究は多く，赤外分光法による研究も多い．

種々の2価カチオンで置換したY型ゼオライトと水の吸着系の赤外吸収スペクトルには，ある程度の共通性がみられる．多くの場合，OH伸縮領域に6～7本の吸収が現われ，3650および3540 cm^{-1}近辺の吸収は触媒活性に寄与する酸性の構造水酸基，3680 cm^{-1}近辺は物理吸着水，3600 cm^{-1}近辺は$M(OH)^+$によるものと考えられている[6]。しかしそれらについての詳細は必ずしも明らかにされてはいない．本報の目的は2価カチオン置換Y型ゼオライトの一例として，Zn-Yをとりあげ，HDOを用いて得られる新しい情報に基づいて各吸収帯を帰属し，その水吸着系の状態を明らかにしようとするものである．

2. 実験方法

2・1 試薬および試料

試薬　D_2OはE. Merck, Darmstadt社製，99.75％のものを，H_2Oは脱イオン蒸留水を用い，それぞれ液体窒素を用い凍結排気を繰り返して脱ガスした．$ZnCl_2$は市販特級試薬を用いた．

試料　Zn-YはNa-Yをイオン交換して作った．Linde Molecular Sieves SK-40（ユニオン昭和KK製，合成Na-Y，Si/Al＝2.3，比表面積770m^2/g）含水物重量約30gに10％$ZnCl_2$溶液（少量のHClを加えて完全に溶かした．pH＝5.15）500mℓを加え，80℃にて24時間反応させた．新しい$ZnCl_2$溶液と交換しながら，この操作を3回くり返した．その後，Cl^-イオンが検出されなくなるまで脱イオン水で洗浄したものをZn-Y試料とした．

得られたZn-Yのイオン交換率を求めるため，試料中のZn^{2+}およびNa^+イオンを，それぞれ蛍光X線分析法および原子吸光法によって定量分析した．その結果98％以上イオン交換されていることが確認された．

この試料のX線回析を測定した結果，そのパターンはBroussardら[4]によって報告されているモレキュラーシーブ13Xのそれに完全に対応し，Y型ゼオライトの結晶構造が保たれていることがわかった．基線が平坦な直線であることから，結晶性は十分に良好であることが確認された．

2・2 実験操作

実験操作は，用いた分光器の違い以外は前報[2,3]と同一であったが，特に前報で触れなかった点について具体的に記述する．

赤外吸収スペクトル測定用試料の調整　一般に粉体表面の赤外吸収スペクトルを透過法によって測定する場合粒子直径が大きいと光の散乱損失が著しく，測定が不可能である．少量の大つぶ粒子が混入しても，透過率は著しく低下するので，通常は粒径を1μm以下にそろえる必要がある．そこで次のようにしてスペクトル測定用試料を調製した．

約5gのZn-Yをアルミナ製の自動らいかい機にとり，これに約10mℓの脱イオン水を加え，蒸発減少分を適時補充しながら約5時間粉砕した．これを脱イオン蒸留水2ℓに良く撹拌分散させ，24時間静置した．ついでその

＊　北海道工業開発試験所第2部2課

上澄液（微粒子懸濁液）だけを取り出し，高速連続遠心分離器で，12000rpm にて微粒子を分離した．この微粒子の直径は，電子顕微鏡で観測した結果，最大約1μmであった。また，微粉末の収率は15% 程度であった．

この微粉末試料を錠剤成型器を用い，2.5 ton/㎠ で加圧して直径20あるいは25㎜の円盤状に成形した後，その両側を切り落して幅 10㎜，長さ 20～25㎜の薄片とし，赤外吸収の測定に供した．この切り落し操作は，10×5×40㎜程のステンレススチール製四角柱と顕微鏡用スライドガラスの間に円盤状薄片をしっかりはさみ，余分な部分をスパチュラで割り落して行った．

赤外測定用セル　用いた赤外測定用セルを **Fig. 1** に示した．これは，Angell ら[5] が考案したのを改良したものである．Angell らは結晶窓板の貼り付けには高真空グリースを，バルブはグリースつき真空コックを用い，試料交換はバルブ部分と本体の間に設けたジョイントの取りはずしによって行っている．しかし，このセルでは真空グリース蒸気によって試料片が汚染されることがわかったので，窓板の貼り付けにはエポキシ系接着剤を用い，バルブはグリスレス・テフロン高真空コックを用いた．本体はパイレックスガラス製で，500℃ までの加熱が可能である．試料交換は，**Fig.1** の *d* 部分を切断し，再溶接することによって行った．この際，バーナー燃焼ガス中の CO_2 がセル内に入ると試料表面に化学吸着して，カルボニル様表面種を生成する* ので，切断部分を完全に密着した状態で炎に入れて再溶接した．セルの枝の部分を小型電気炉に入れて，試料片を加熱した．スペクトルの測定は，セルを傾斜させ試料片を窓の部分に滑り落して行った．

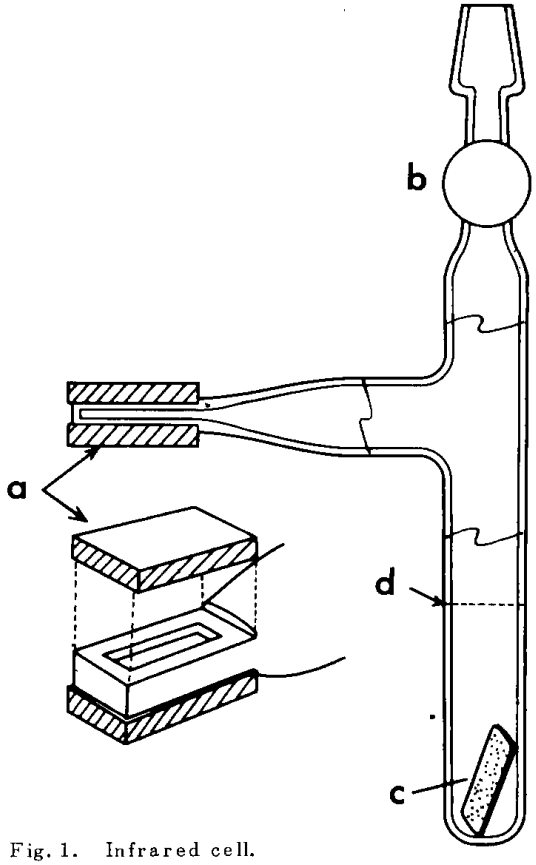

Fig. 1. Infrared cell.
a, KBr windows. b, Teflon greaseless valve. c, Sample piece.
d. Position to be cut.

赤外スペクトルの測定には JASCO, 402-G および DIGILAB, FTS-15B 型を用いた．後者による実測値を基準とし，OH 伸縮（4000～3400cm^{-1}）および変角（1800 1300 cm^{-1}）波数領域には水蒸気およびアンモニアガスを，OD 伸縮領域（2800～2300cm^{-1}）には臭化水素ガスを用いて，前者による実測値の波数を補正した．

HDO 吸着系の OH 伸縮および HOD 変角振動領域の測定には，H_2O : D_2O = 1 : 5 モル比の混合水（この組成はおよそ，H_2O : HDO : D_2O = 1 : 10 : 25である）を用い同じく OD 伸縮領域の測定には，H_2O : D_2O = 3 : 1 の混合水（H_2O : HDO : D_2O = 9 : 6 : 1）を用いた．

3. 実 験 結 果

3・1 吸着過程のスペクトル

3・1・1 H_2O, D_2O 吸着系

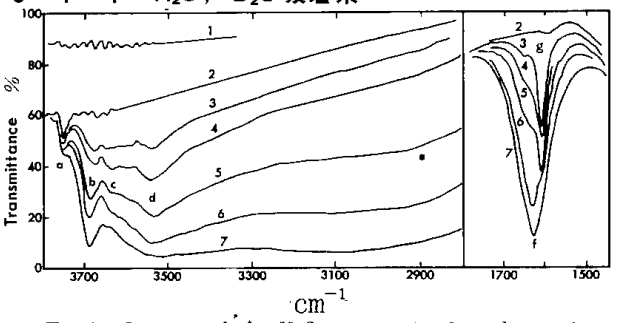

Fig. 2. Spectra of the H_2O system in the adsorption process.
(1) Blank cell. (2) Evacuated at 500℃ for 3h. (3) 6.1, (4) 12.2, (5) 18.3, (6) 24.4, (7) 30.5 mℓ (stp)/g of H_2O vapor were readsorbed. Sample piece thickness 14mg/㎠.

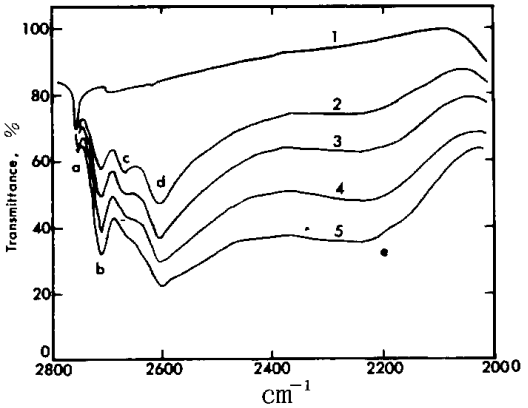

Fig. 3. Spectra of the D_2O system in the adsorption process.
(1) Evacuated at 500℃ for 3h. (2) 5.0, (3) 10.0, (4) 15.0, (5) 20.0 mℓ (stp)/g of D_2O vapor were readsorbed. Sample piece thickness 14 mg/㎠

＊通常この表面種は1400cm^{-1}近辺に吸収を示し 500℃ の加熱排気によっても脱離しない。

吸着量を段階的に増しながら，0～30mℓ (STP)/g の範囲内で，Zn-Yと H_2O および D_2O の吸着系のスペクトルを測定した。これらを **Fig.2** および **Fig.3** に示した．図に見るように，水 (H_2O, D_2O) の吸着によって OH(OD) 伸縮領域には4本の吸収が現われた．H_2O の場合 (**Fig.2**) と D_2O の場合(**Fig.3**)のこれらの吸収は，完全に対応させ得るものであり，それぞれ対応する吸収帯の波数比は 1.36 前後であった．このことから，これらの吸収は全て OH あるいは OD の振動によるものであることがわかる．これら4本の吸収にそれぞれ，b, c, d, eの記号を付した．a 吸収帯は，各種のゼオライトに認められ，500℃ 排気によっても消失しない吸収で，ゼオライトに不純物として含まれる SiO_2 の表面 OH 基によるものとされている。

OH 変角領域には g および f の2本の吸収が現われた。g は鋭く，比較的吸着率の低い時に現われ，吸着率の増加と共に巾の広い f 吸収の増加が顕著になるのが図からわかる。

各吸収帯の実測波数値を他の系のそれらとともに**Table 1** に示した．

Table 1. Summery of the IR bands of Zn-Y Zeolite-water system

Band sign	D_2O system [cm^{-1}]	H_2O system [cm^{-1}]	HDO system (cm^{-1}) Stretching regions OD	Stretching regions OH	Deformation region
		[in the adsorption process]			
a	2762	3743	2762	3745	
b	2717	3685	2677	3685	
c	2675	3635		3640	
d	2615	3538	2615	3540	
e	2200	2900	2240	3200	
f		1625			
g		1610			
h				2910	
k					1500
l					1460
m					1427
		[in the desorption process]			
a	2762	3743	2762	3745	
c	2682	3640	2682	3640	
d	2615	3535	2615	3535	
h				2925	
p	2702	3667	2702	3667	
q		1655			
r		1615			
s					1480
t					1430
u					1410
w	2445	3300			
x	2260	2950	2270	3130	

3・1・2 HDO 吸着系

HDO-Zn-Y 吸着系の OH 伸縮および変角振動領域のスペクトルを **Fig.4** に，OD 伸縮領域のそれを **Fig.5** に示した．図に見るように，伸縮振動領域のスペクトル

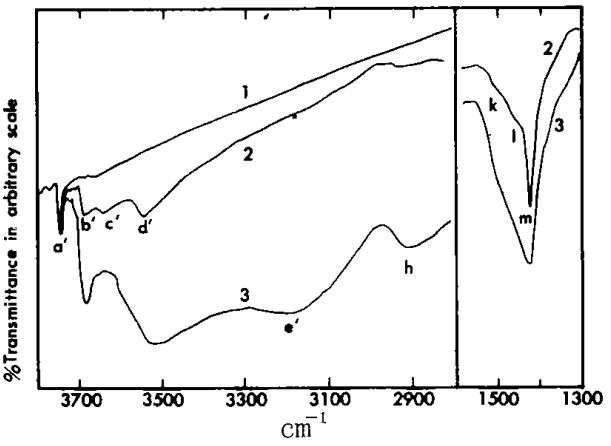

Fig. 4 Spectra in the OH stretching and deformation regions of the HDO system in the adsorption process.
(1) Evacuated at 500℃ for 3h. (2) 9.2, (3) 27.6 ml(stp)/g of the vapor of H_2O-D_2O 1 to 5 mixed water were readsorbed. Sample piece thickness 18 mg/cm^2. The spectra in the deformation region were obtained by rationing the observed spectra against that of the sample after 500℃ evacuation.

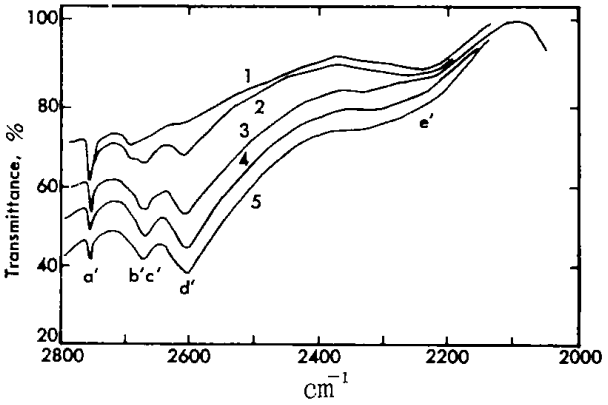

Fig. 5 Spectra in the OD stretching region of the HDO system in the adsorption process.
(1) Evacuated at 500 ℃ for 3h. (2) 4.6, (3) 9.2, (4) 13.8, (5) 18.4 ml (stp)/g of the vapor of H_2O-D_2O 3 to 1 mixed water were readsorbed. Sample piece thickness 40 mg/cm^2.

は H_2O (D_2O) の場合 (**Fig.2, 3**) と類似したものであり，e 吸収が高波数シフトを示し，また OH 領域に新たな h 吸収が現われた以外は，**Fig. 2, 3** における b, c, d と同一波数の位置に，対応する b′, c′, d′ の吸収が認められた．しかし，OD 領域ではこの b′ に相当する吸収は認められない．**Fig. 3** の c, d 吸収，**Fig. 5** の c′, d′ 吸収の強度を比較すると，相対的に c′ の吸収が大きいことから，**Fig. 5** の b′吸収は c′ に重なっているものと考えられる．また h 吸収も OD 領域には認められない．

変角振動領域には，H_2O の場合2本であったのに対し

て，k，l，mの3本の吸収が出現した（**Fig. 4**）．このうちmは鋭く，かつ吸着率の低い時に顕著であるので，**Fig. 2** のgに対応し，k，lは比較的に吸着量の多い段階で強度増加を示すので同じくfに対応するものと考えられる．

3・2　脱離過程のスペクトル

3・2・1　H_2O, D_2O 系

Fig. 6 および **Fig. 7** は，段階的に昇温排気して測定したH_2O系およびD_2O系のスペクトルである．

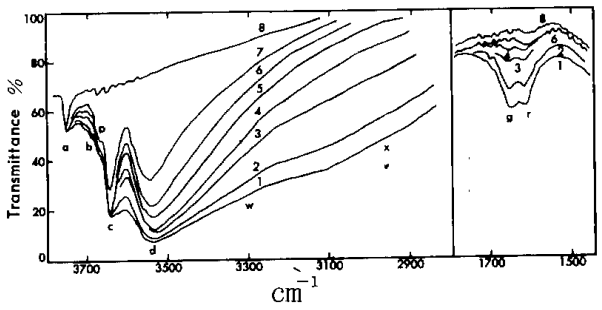

Fig. 6　Spectra of the H_2O system in the desorption process. Evacuated at (1) 90 ℃ for 1h, (2) 120 ℃ for 1h, (3) 165 ℃ for 30 min, (4) 185 ℃ for 30 min, (5) 215 ℃ for 1h, (6) 253 ℃ for 30 min, (7) 300 ℃ for 40 min, (8) 500 ℃ for 3h after exposure to the H_2O vapor. Sample piece thickness 14 mg/cm².

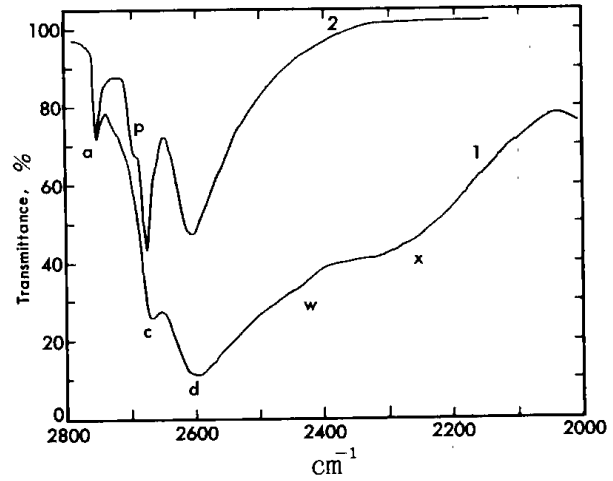

Fig. 7　Spectra of the D_2O system in the desorption process. Evacuated at (1) 90 ℃ for 1h 30 min, (2) 300 ℃ for 45 min after exposure to the D_2O vapor. Sample piece thickness 14 mg/cm².

伸縮振動領域に6本の吸収が認められるが，このうちa、b，c，d吸収は吸着過程のスペクトルにおける同符号の吸収にそれぞれ対応することは明らかである．吸着過程のスペクトルに比べcおよびd吸収が著しく強大であるのが特徴的である．またc吸収に近接して新たな吸収pが認められた．b吸収は90℃，1hの排気で，吸収帯として検知できない程度にまで減少している。

吸着水によると考えられる伸縮振動は，ほぼ伸縮領域の全域にわたる広大な吸収として観測されるが，H_2O系では2950 cm^{-1}近辺に，D_2O系では2250 cm^{-1}近辺に吸収の極大が認められる．

変角領域には，吸着過程の場合と同様，2本の吸収（g，r）が認められるが，波数，形ともに前者とは異ったものであることがわかる．これらの吸収は，排気温度の上昇に伴い，ほぼ同じ割合で強度減少を示した。

3・2・2　HDO 系

Fig. 8 および **9** は，**Fig. 6**，**7** と同様の条件下で測定したHDO系のスペクトルである．

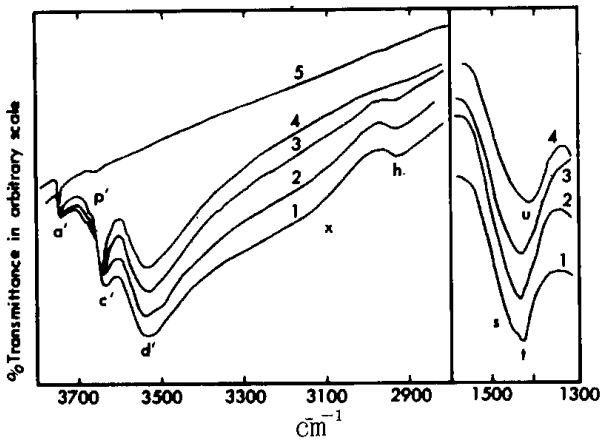

Fig. 8　Spectra in the OH stretching and deformation regions of the HDO system in the desorption process.
Evacuated at (1) 90 ℃ for 1h 10 min, (2) 120 ℃ for 50 min, (3) 165 ℃ for 30 min, (4) 200 ℃ for 1h, (5) 500 ℃ for 3h after exposure to the vapor of H_2O-D_2O 1 to 5 mixed water. Sample piece thickness 18 mg/cm². The spectra in the deformation region were obtained by rationing the observed spectra against that of the sample after 500 ℃ evacuation.

これらの伸縮領域を **Fig. 6** および **7** と比較すると非常によく似ていることがわかる．**Fig. 6**，**7** のa，p，c，dに対応するa′，p′，c′，d′の吸収は，それぞれ全く同一波数を示した．吸着水の伸縮振動と考えられる吸収は極めて巾が広いため，そのピーク位置は明確ではないが，OD 伸縮領域ではほぼ同位置に，OH 伸縮領域では3130 cm^{-1}近辺に認められる．また吸着過程（**Fig. 4**）の場合と同様に，2925cm^{-1}にh吸収が認められる．

HOD 変角領域の吸収は相互に重なり合っているため明確には判断できないが，1480 cm^{-1}（s），1430 cm^{-1}（t）近辺および1410 cm^{-1}（u）の3本の吸収が現われていると見ることができる．

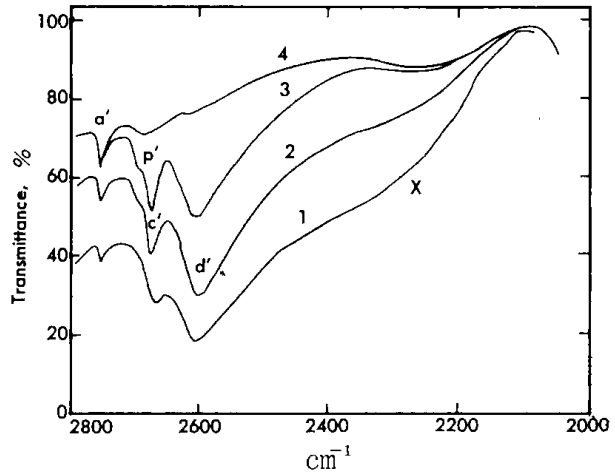

Fig. 9 Spcetra in the OD stretching region of the HDO system in the desorption process. Evacuated at (1) 90 ℃ for 1h, (2) 165 ℃ for 30 min, (3) 300 ℃ for 45 min, (4) 500 ℃ for 3h after exposure to the vapor of the H_2O-D_2O 3 to 1 mixed water. Sample piece thickness 40 mg/cm^2.

4．考　　察

吸収帯 p，c および dは，H_2O および D_2O 系と HDO 系のそれぞれ対応する領域において完全に同一波数を示すので，ゼオライト表面の構造 OH 基によるものである．前報[3] で，Na-Y と水の吸着系にもこの c および d とほぼ同位置に吸収帯があり，これらが吸着水によるものであることを示したが，Zn−Y 系の c，d 吸収は，これらとは全く別のものであることが，HDO の使用によって明らかになった．これら p，c，d の吸収が，加熱排気過程のスペクトルで，より強大であったが，室温吸着過程のスペクトルにも相当量観測されたことは，水の解離吸着によるこれらの構造 OH 基の生成反応が室温でも起こり，加熱により更に進行することを示す．しかし 500 ℃ 排気でほぼ完全に消失しており，ある温度以上では脱離し減少する．この脱離開始温度は，吸着水分子の吸収がこれらの吸収帯と重なっているため，明確ではないがスペクトルの変化から 180 ℃ 前後と推定される．

吸着過程のスペクトルに明確に見られる b 吸収帯は，OD 伸縮領域で D_2O 系と HDO 系とで 40 cm^{-1} のシフトを示した．従ってこの吸収は吸着水に基づくものである．この吸着水 **Type I** は，前報[2] で示した非対称的な吸着水(WX-I)と同種のものであり，前報における b, e 吸収帯に，本報の b，e 吸収帯がそれぞれ対応するものと考えられる．2本の HOH 変角振動のうち f が HDO 系で2本に分裂していることから，これが **Type I** 吸着水に帰せられる．もう1本の HOH 変角振動 g は HDO 系の m に対応し，両系で1本づつであることから，これは C_{2v} の形を保って吸着している水分子によるものと考えられる(**Type II**)。この吸着水に帰属し得る伸縮振動は，H_2O，D_2O および HDO のいずれの系のスペクトルにも明らかには認められない．しかし別に FTIR を用いて H_2O および HDO の OH 伸縮領域で吸着過程の差スペクトルを測定した結果，いずれの系においても 3500 cm^{-1} 近辺に比較的巾の広い吸収帯が認められ，この吸収帯がこの型の吸着水に対応するものと考えられる．

脱離過程のスペクトルにも2種類の吸着水が見られたが，これらはそのスペクトルの相異からいずれも上記のものとは異った状態にあることがわかる．しかしその詳細についてはスペクトルが不鮮明である上，ほぼ同時に脱離減少するので吸収帯の分離ができず，不明である．室温吸着した水は言はば準安定な状態にあり，加熱によってより安定な状態に変化するものと考えられる．

H_2O 系および D_2O 系の脱離過程のスペクトルに見られる 3300 cm^{-1} (**Fig. 6**), 2445 cm^{-1} (**Fig. 7**) の弱い吸収 (w) は対応する HDO 系の各領域には認められず，前報[2),3)] において他のゼオライトと水の吸着系にもほぼ同波数に見られ，吸着 H_2O および D_2O の倍音変角振動に帰属できる．h 吸収帯も他のゼオライト−HDO 系[2,3)] に認められており，吸着 HDO 分子の倍音変角あるいは何らかの結合音によるものと考えられる．

b 吸収帯は，OD 伸縮領域においては，D_2O と HDO とで 40 cm^{-1} のシフトを示したが，対応する OH 伸縮領域では検知し得るほどのシフトを示さなかった．同様の事実は前報[2,3)] の Na-X の吸着水，Na-Y の2種類の吸着水でも観測されている．その理由は，現在のところ全く不明であるが，これらの事実は HDO を用いて，ある吸収が構造水酸基によるものか水分子によるものかを判定する場合，D_2O 系と HDO 系の OD 伸縮を比較する方が有利であること，少くとも H_2O 系と HDO 系の OH 伸縮領域の比較だけでは誤った結論を導きかねないことを示唆している．

参考文献

1) 三上康子，日野雅夫，日本化学会，日本分析化学会北海道支部 1977 年冬季研究発表会講演要旨集，P 53 (1977)
2) Masao Hino, Bull. Chem. Soc. Jpn., 50, 574 (1977)
3) 日野雅夫，三上康子，日本化学会第36春季年会，講演予稿集 I，P 344 (1977)
4) L. Broussard and D.P. Shoemaker, J. Am. Chem. Soc., **82**, 1041 (1960)
5) C. L. Angell and P.C. Schaffer, J. Phys. Chem., **69**, 3463 (1965)
6) 例えば，原，高橋編，“ゼオライト−基礎と応用” 講談社 (1970)

Infrared Studies on Water Adsorption Systems with the Use of HDO

Ⅲ. Zn-Y Zeolite

Masao HINO and Yasuko HIRAMA

Infrared spectra of Zn-Y Zeolite-H_2O, $-D_2O$, and $-HDO$ systems were measured in the adsorption and desorption processes. As a result, the followings were elucidated. There are three kinds of structural hydroxyl groups on the surface of Zn-Y Zeolite, which gives absorption bands at 3667, 3640, and 3535 cm^{-1}, respectively. These hydroxyl groups are produced by the adsorption of water at room temperature on the Zeolite evacuated at 500℃. Heat treatment at higher temperatures promotes the reaction of the groups formation. But the groups are reduced in quantity at temperatures higher than about 180℃ and disappears by evacuation at 500℃.

Two kinds of adsorbed water are formed on the adsorption of water at room temperature. One of which, giving bands at 3685, 2900, and 1625 cm^{-1}, is of the asymmetric type which is analogous to those on the systems of Na-X and Na-Y Zeolites. The other, giving bands at 3500 and 1610 cm^{-1}, is that of adsorbed in the symmetric mode. Two kinds of adsorbed water are also observed in the desorption process. But, both of them are in different states from those in the adsorption process.

It was emphasized that comparison of the spectra must be made not only in the OH stretching region between H_2O system and HDO system, but also in the OD stretching region between D_2O system and HDO system to determine whether a band arose from a structural hydroxyl groups or from adsorbed water molecules.

北海道工業開発試験所報告
第 19 号

昭和54年3月30日　印刷
昭和54年3月30日　発行

発行所　工業技術院北海道工業開発試験所
札幌市豊平区東月寒41－2
電話　011（851）0151
印刷所　協進印刷株式会社
札幌市東区北23条東7丁目
電話　011（751）3860

REPORTS OF
THE GOVERNMENT INDUSTRIAL DEVELOPMENT LABORATRY, HOKKAIDO

No. 19 March 1979

Contents

Published by

The Government Industrial Development Laboratory, Hokkaido
41-2, Higashi-tsukisamu, Toyohira-ku, Sapporo, Japan